Published in final edited form as:

Mol Cell. 2008 February 01; 29(2): 191–206. doi:10.1016/j.molcel.2007.11.026.

Functional Anatomy of Phospholipid Binding and Regulation of Phosphoinositide Homeostasis by Proteins of the Sec14 Superfamily

Gabriel Schaaf[1,5], **Eric A. Ortlund**[2,3,5], **Kimberly R. Tyeryar**[1], **Carl J. Mousley**[1], **Kristina E. Ile**[1], **Teresa A. Garrett**[4], **Jihui Ren**[1], **Melissa J. Woolls**[1], **Christian R.H. Raetz**[4], **Matthew R. Redinbo**[2,3], **Vytas A. Bankaitis**[1,*]

[1]Department of Cell and Developmental Biology, School of Medicine, Lineberger Comprehensive Cancer Center, University of North Carolina at Chapel Hill, Chapel Hill, NC 27599-7090, USA

[2]Department of Chemistry, School of Medicine, Lineberger Comprehensive Cancer Center, University of North Carolina at Chapel Hill, Chapel Hill, NC 27599-7090, USA

[3]Department of Biochemistry and Biophysics, School of Medicine, Lineberger Comprehensive Cancer Center, University of North Carolina at Chapel Hill, Chapel Hill, NC 27599-7090, USA

[4]Department of Biochemistry, Duke University Medical Center, Durham, NC 27710, USA

[5]These authors contributed equally to this work.

SUMMARY

Sec14, the major yeast phosphatidylinositol (PtdIns)/phosphatidylcholine (PtdCho) transfer protein, regulates essential interfaces between lipid metabolism and membrane trafficking from the trans-Golgi network (TGN). How Sec14 does so remains unclear. We report that Sec14 binds PtdIns and PtdCho at distinct (but overlapping) sites, and both PtdInsand PtdCho-binding activities are essential Sec14 activities. We further show both activities must reside within the same molecule to reconstitute a functional Sec14 and for effective Sec14-mediated regulation of phosphoinositide homeostasis in vivo. This regulation is uncoupled from PtdIns-transfer activity and argues for an interfacial presentation mode for Sec14-mediated potentiation of PtdIns kinases. Such a regulatory role for Sec14 is a primary counter to action of the Kes1 sterol-binding protein that antagonizes PtdIns 4-OH kinase activity in vivo. Collectively, these findings outline functional mechanisms for the Sec14 superfamily and reveal additional layers of complexity for regulating phosphoinositide homeostasis in eukaryotes.

*Correspondence: vytas@med.unc.edu.

Supplemental Data

Supplemental Data include Supplemental Experimental Procedures, seven figures, and one table and can be found with this article online at http://www.molecule.org/cgi/content/full/29/2/191/DC1/.

Accession Numbers

PDB codes are described as follows: Sec14 homolog Sfh1 in complex with PtdEtn (3B74); Sec14 homolog Sfh1 in complex with PtdIns, with the 18:0/ 18:1 molecular species modeled (3B7N); Sec14 homolog Sfh1 in complex with PtdCho (16:0/18:1 molecular species) (3B7Q); and Sec14 homolog Sfh1 in complex with PtdIns and PtdCho (3B7Z). For 3B7Z, the data are from crystals composed of a mixture of Sfh1::PtdIns and Sfh1::PtdCho unit cells. The stoichiometry of unit cells within the crystals is 60%:40%.

INTRODUCTION

Eukaryotic cells compartmentalize membrane surfaces so that biochemical reactions with signaling power are registered in a spatially and temporally informative manner. Phosphorylated derivatives of phosphatidylinositol (PtdIns), termed phosphoinositides (PIPs), are known components of such membrane-associated signaling systems in eukaryotes (Majerus, 1997; Fruman et al., 1998; Strahl and Thorner, 2007). The diversity of PIP signaling is widely appreciated and, in part, derives from chemical heterogeneity of PIP species. That is, distinct PIPs form chemically unique membrane platforms on which specific biological reactions take place. In addition to the information defined by PIP identity, however, there exist additional layers of functional specification for PIP signaling. Such regulatory layers are revealed by demonstrations that production of an individual PIP by a particular PtdIns kinase still yields distinct outcomes in a single cell (Routt et al., 2005). Mounting evidence points to PtdIns/PtdCho-transfer proteins (PITPs) as intrinsic components of biochemical nanoreactors that determine outcomes for PIP signaling (Ile et al., 2006). Understanding how PITPs channel PtdIns to PtdIns kinases is central to an understanding of how PIP synthesis/signaling is regulated.

Sec14, the major yeast PITP, coordinates phospholipid (PL) metabolism with vesicle formation on yeast TGN membranes (Cleves et al., 1991a; Li et al., 2002). It is also the prototype for the uniquely eukaryotic Sec14-protein superfamily (>500 members; Phillips et al., 2006). Sec14-superfamily diversity, when coupled with multiplicity of Sec14-like proteins in even simple cells, reports high degrees of functional specification for these proteins. Given emerging evidence that Sec14-like proteins specify outcome for PtdIns kinase action (Routt et al., 2005), Sec14-superfamily diversity has direct implications for mechanisms of functional diversification of PIP signaling. Consistent with this idea, the biological importance of Sec14 proteins is emphasized by the deranged membrane trafficking and lipid metabolism that accompany defects in members of this superfamily (Bankaitis et al., 1989, 1990; Cleves et al., 1991b; Skinner et al., 1995; Xie et al., 1998; Rivas et al., 1999; Yanagisawa et al., 2002; Vincent et al., 2005). Moreover, Sec14-like protein deficiencies underly inherited human disorders (Ouachi et al., 1995; Aravind and Koonin, 1999; Benomar et al., 2002; Bomar et al., 2003; Meier et al., 2003; D'Angelo et al., 2006).

Sec14 offers a facile model for addressing mechanisms for how members of the Sec14 superfamily regulate lipid metabolism and PtdIns kinases. How Sec14 binds PtdIns and PtdCho, how Sec14 executes PtdIns/PtdCho exchange, and how individual PtdIns- and PtdCho-binding activities contribute to Sec14 function and PtdIns kinase activation remain unknown. Herein, we report yeast Sfh1 (the closest Sec14 homolog; Li et al., 2000) and Sec14 bind PtdCho and PtdIns at distinct sites and that PtdIns- and PtdCho-binding activities are each essential biological Sec14 properties. We further show both binding activities must reside on the same protein molecule to generate a biologically functional Sec14 and that each activity is required for Sec14-mediated regulation of PIP homeostasis in vivo. The data are most consistent with an interfacial presentation mechanism for Sec14 function, and this mechanism fortifies Pik1 PtdIns 4-OH kinase activity in the face of an oxysterol-binding protein that antagonizes Pik1 in vivo. These discoveries clarify mechanisms for how Sec14

regulates PIP metabolism in cells, report new layers of complexity in regulation of PIP homeostasis, and forecast a remarkable versatility for proteins of the Sec14 superfamily in regulation of the lipid signaling landscape of eukaryotic cells.

RESULTS

PL-Bound Sfh1 Defines a Closed Conformer

The original Sec14 crystal structure is that of an apo-Sec14, in a presumptive “open” conformation, where bound PL was displaced by the β-octylglucoside required for crystallization (Sha et al., 1998; Phillips et al., 1999). As such, that apo-Sec14 structure fails to clarify how Sec14 binds its physiological PL ligands. We now report the binding problem is solved by structural analyses of the closest Sec14 homolog—the yeast Sfh1. Recombinant Sfh1 was crystallized, and its structure was determined at1.9 Å resolution (Table 1). This structure describes a PtdEtn-bound holo-Sfh1 (see below) and consists of 11 α helices, 5 short 3_{10} helices, and 6 β strands. The general features of the refined structure are similar to those determined for the open β-octylglucoside-bound Sec14 conformer (Figure 1A). Sfh1 shares 62.3% sequence identity with Sec14 and displays an rmsd of 3.1Å over 292 equivalent C α positions (Maiti et al., 2004). The first four helices (A1–A4) comprise the tripod motif, while the core of the Sfh1 fold consists of a central six-stranded β sheet sandwiched between three α helices and the C-terminal string motif.

The most striking difference between the Sfh1::PtdEtn structure and the apo-Sec14 structure of Sha et al. (1998) is repositioning of the Sfh1 A9/T3 structural element (A10/T4 in Sec14) (Figures 1B and 1C). In the Sfh1 structure, the C terminus of helix A9/T3 is displaced ~17.5Å toward helix A8 (A9 in Sec14) from the position apparent in the open Sec14 conformer—thus closing the PL binding pocket. The closed conformation of A9/T3:A10 is stabilized by hydrophobic contacts with helix A8, β strand B5, and interactions with *sn*-1 acyl chain of bound PL. Three residues from helix A9/T3 (F223, F227, and V230), one (L234) from the loop that bridges helix A9/T3 with helix A10, and one from helix A10 (T238) also directly contact the acyl chains of bound PtdEtn. These Sfh1 residues are all conserved in Sec14 other than V230, whose counterpart in Sec14 is F228.

The holo-Sfh1 structure rationalizes the strict conservation among Sec14-like proteins of the gating helix (Sfh1 A9/T3; Sec14 A10/T4) KPFL motif. Residue P232 terminates helix A9/T3 and positions F233 for interaction with K197 on helix A8 (R195 in Sec14). The K197-F233 interaction (R195-F231 in Sec14) stabilizes the closed conformation. Helices A9/T3 and A10 are Sfh1 cognates of the Sec14 helical gate that regulates access to the Sec14 hydrophobic cavity (Ryan et al., 2007). Both helices contact bound PL (Sfh1 residue L234 of the KPFL motif contacts the *sn*-1 acyl chain of bound PL). Comparisons of Sfh1 and Sec14 structures project nearly all Sec14 residues that correspond to Sfh1 residues that interact with bound PL are also capable of stabilizing the ,gating helix.-

Crystal Structures for Sfh1 Bound to Amino PLs

Sfh1 purified from *E. coli* is bound to PtdEtn, and mass spectrometry of lipophiles extracted from Sfh1 crystals confirms the crystallizing unit as an Sfh1::PtdEtn complex (Schaaf et al.,

2006). Consistent with these analyses, electron density within the Sfh1 PL-binding pocket prominently features an 8σ tetrahedral peak with two distinct tails protruding toward the surface. A single saturated PtdEtn molecule was refined into the clear $F_o - F_c$ difference electron density observed in the Sfh1 hydrophobic cavity (Figure 2A). The electron density allowed assignment of 14 and 15 carbons for the *sn*-1 and *sn*-2 acyl chains of bound PtdEtn, respectively. As a 14:0/15:0 PtdEtn is not a natural PL (unless the 15 carbon *sn-2* acyl chain harbors a cyclopropane [cp] moiety), the observed electron density was likely limited by disorder in headgroup-distal acyl chain regions. Analyses of PL from Sfh1::PtdEtn crystals indicate a family of bound PtdEtn molecular species range from 30:0 to 37:1cp species (Schaaf et al., 2006). PtdEtn engages in van der Waals contacts with 14 residues, and the phosphate moiety is coordinated by the side-chain −OH groups of residues S175 and T177, whereas the ethanolamine (Etn) nitrogen resides within 2.6 Å of the phenolic oxygen of Y113 (Figure 2B). A remarkable feature is the depth at which the PtdEtn headgroup is buried in the Sfh1 cavity, occupying the core of the protein ~17.5Å from the solvent-accessible surface of Sfh1 (Figure 1A).

Crystals of Sfh1 loaded with 16:0/18:1 PtdCho were grown. Negative-ion ESI-MS of organic extracts of Sfh1::PtdCho crystals highlighted a major ion (m/z 794.55) corresponding to a chloride adduct of 34:1 PtdCho (Figure S1 available online). Collision-induced decomposition mass spectrometry (CID-MS) confirmed the assignment as 16:0/18:1 PtdCho. The Sfh1::PtdCho structure was determined at 2.0 Å (Table 1), and electron density within the Sfh1 pocket reveals one bound 16:0/18:1 PL with a new tetrahedral peak corresponding to the trimethylated nitrogen of the choline (Cho) headgroup (Figure 2C). The electron density supports placement of acyl chains in their entirety, and as expected, PtdCho and PtdEtn are similarly coordinated. PtdCho makes extensive contacts with residues along the entire face of the β sheet and along helices A8–A10 that gate the Sfh1 pocket—27 residues are in van der Waals contact with bound PtdCho. As PtdEtn and PtdCho are zwitterionic PLs with a net neutral charge, rather weak interactions with the S175 and T177 −OH groups are sufficient to stabilize the phosphate moiety of either PL. In the absence of an Etn headgroup nitrogen to H bond with Y113, the Cho headgroup is stabilized by cation-π interactions with Y124 and Y153 (Figure 2D).

Ordered H_2O Molecules Are Sequestered within the Sfh1 Hydrophobic Cavity

Sfh1::PtdEtn and Sfh1::PtdCho exhibited differences in the volumes of their respective PL binding cavities. In the case of Sfh1:: PtdEtn, the hydrophobic cavity volume is 2695.3 $Å^3$, whereas the volume of bound 14:0/15:0 PtdEtn is 1794.8 $Å^3$. For Sfh1::PtdCho, the respective volumes are 3068.7 $Å^3$ and 2006.1 $Å^3$. Ordered H_2O molecules account for the volume differences in both circumstances. The Sfh1::PtdEtn and Sfh1::PtdCho structures report six and five H_2O molecules within the cavity, respectively (Figures 2A and 2C). For Sfh1::PtdCho, the five ordered H_2O molecules are coordinated within 2.7–3.9 Å of the headgroup-distal region of the *sn*-2 acyl chain of bound PtdCho.

The Sfh1::PtdCho structure reveals the side chains of Y109, Q111, Y124, and E126 protrude from the β sheets that form the floor of the hydrophobic PL binding pocket and organize a hydrophilic surface on the pocket floor (Figure 2E). These same residues coordinate ordered

H_2O in the region of the binding pocket adjacent to C5 of the PtdCho *sn*-2 acyl chain. These data explain the paradoxical electron spin resonance (EPR) results that reported the headgroup-proximal region of the *sn*-2 acyl chain of Sec14::PtdCho exhibits a protic, yet solvent-inaccessible, signature (Smirnova et al., 2006, 2007).

Structure of the Sfh1::PtdIns Complex

To elucidate structural determinants of PtdIns binding, Sfh1 was loaded with soybean PtdIns, crystallized and the structure was solved to 1.86 Å resolution (Table 1 and Figure 3A). PtdIns (modeled as the 18:0/18:1 molecular species) is incorporated into the Sfh1 binding cavity in an orientation strikingly distinct from that resolved for amino PLs (Figure 3A; see below). Rather than sequestering PtdIns deep within the Sfh1 cavity, the inositol (Ins) headgroup is coordinated near (yet beneath) the protein surface. The glycerophospho-Ins moiety of bound PtdIns forms extensive contacts with helix A10 located C-terminal to the helical gate and with loops between helices A2 and A3, β strand 2–helix A_8, and helices A9/T3–A10. These Sfh1-PtdIns interactions involve 11 H bonds distributed across the PtdIns backbone and head-group region (Figures 3B and 3C). The headgroup phosphate is coordinated by the main-chain amide nitrogens of E209, R210, and M211 and the side chain −OH of T238 and is neutralized by a 2.7 Å electrostatic interaction with the K241 side chain. The −OH groups on the Ins ring H bond with the side chains of R61, D235, and E209 and the Q204 main-chain carbonyl. In addition, Sfh1 K_{62} forms H_2O-mediated contacts to two Ins –OH groups.

Previous data showed dual conversion of Sec14 residues K66 and K239 to Ala (K62 and K241 in Sfh1) specifically compromises PtdIns binding. It was suggested these residues, along with E207 (Sfh1 E209), engage in specific binding of the PtdIns headgroup by Sec14 (Phillips et al., 1999). The Sfh1 data validate and sharpen that hypothesis. The Sfh1::PtdIns structure demonstrates Sec14 residue K239 (K241 in Sfh1) coordinates the PtdIns headgroup phosphate, rather than the Ins ring, as previously inferred by Phillips et al. (1999). The investment by Sfh1 in an extensive network of H bonds and van der Waals contacts in PtdIns binding suggests a rationale for the hierarchy in PL binding affinity attributed to Sec14-like PITPs (i.e., PtdIns > PtdCho).

The distal regions of Sfh1-bound PtdIns acyl chains are configured similarly to those of bound PtdEtn and PtdCho, and PtdIns engages in van der Waals contacts with 30 Sfh1 residues. The respective PL-binding pocket and bound 16:0/18:2 PtdIns volumes are 4050.6 $Å^3$ and 2204.2 $Å^3$. Unlike Sfh1::PtdEtn and Sfh1::PtdCho, the excess cavity volume for Sfh1::PtdIns relative to ligand volume does not derive from sequestration of ordered H_2O in the hydrophobic cavity. It results from confluence of an H_2O-filled cleft formed primarily by the tripod motif (helices A1–A4), with the PL binding cavity.

Analysis of Crystals Containing Sfh1::PtdCho and Sfh1::PtdIns

The dissimilarity for how Sfh1 binds PtdCho versus PtdIns is dramatically illustrated in analyses of Sfh1 crystals obtained after Sfh1::PtdEtn was incubated with liposomes composed of a 60:40 molar ratio of PtdCho:PtdIns. The crystal structure of ,exchanged-Sfh1 was solved to 2.03 Å resolution (Table 1). Unexpectedly, the electron density maps

exhibit overlapping density for both PtdCho and PtdIns and are characterized by two tetrahedral peaks at 6σ and 6.6σ for the PtdCho and PtdIns phosphate moieties, respectively (Figures 3D and 3E). The PtdIns and PtdCho headgroup phosphates are separated by 8.2 Å in the Sfh1 PL-binding cavity. PtdIns and PtdCho orientations in Sfh1 and the apo-Sec14 structure are presented in Figure S2. In Sfh1, the bound PtdIns molecule is buried in the structure and is shielded from solvent by the R62 side chain and the helical gate. R62 rotamers could plausibly expose the PtdIns headgroup to solvent. Helical gate opening would further expose PtdIns (Figure S2).

Given Sfh1 accommodates only a single bound PL, the structural data represent a composite of both Sfh1::PtdCho and Sfh1::PtdIns unit cells present in the same crystal. There are no obvious backbone conformational differences between Sfh1::PtdCho and Sfh1::PtdIns in the mixed crystals; each asymmetric unit contains one Sfh1::PL complex in the refined model. The final PL occupancy values refined to 60%:40% PtdCho:PtdIns—i.e., a ratio equivalent to the PL stoichiometry presented to Sfh1 during exchange.

Bound PLs Are Immobilized in the Sfh1 Cavity

A property of all holo-Sfh1 structures is the well-ordered acyl chain status within the PL-binding pocket. In all cases, the *sn*-1 acyl chain is better ordered than the *sn*-2 chain of bound PL. For PtdEtn, PtdCho, and PtdIns, the average *sn*-1 acyl chain B factors are 5.8, 9.3, and 6.4 $Å^2$ lower than those of the corresponding *sn*-2 acyl chain. The average B factors for bound PtdEtn, PtdCho, and PtdIns are 30.7, 43.0, and 27.8 $Å^2$, whereas the corresponding B factors for Sfh1 in each complex are 23.5, 23.5, and 22.3 $Å^2$, respectively. These parameters report highly restricted mobility of PL acyl chains within the binding pocket—in agreement with electron paramagnetic resonance (EPR) studies of Sec14::PtdCho (Smirnova et al., 2006, 2007). One exceptional feature is the extent to which the PtdIns headgroup is immobilized. This moiety displays lower average B factors (18.3 $Å^2$) than does protein in Sfh1::PtdIns (22.3 $Å^2$), reflecting the 11 H bonds and the K241 electrostatic interaction invested by Sfh1 in PtdIns headgroup binding.

Design Strategy for Sfh1 and Sec14 Mutants with Defects in PL Binding

The structural data guided design of Sfh1 derivatives with predictable defects in PL binding. Sfh1 residues L179, I196, and V199 line the hydrophobic tunnel, which envelops the acyl chains of bound PtdCho or PtdIns in holo-Sfh1 (Figure S3A). To investigate the general role of PL binding, a ,pinch- mutant was generated where Sfh1 L179 and I196 were both mutated to Trp to sterically obstruct acyl-chain space and prohibit PL incorporation into the Sfh1 cavity (Sec14 pinch mutant is $Sec14^{M177W,V194W}$). Mutant Sfh1s exhibiting steric or electrostatic incompatability with PtdIns headgroup phosphate binding were created by introducing Trp or Asp for T238 and substituting the Ins headgroup H bond partner R61 with Ala (Figure S3B). The cognate Sec14 variants are $Sec14^{R65A,T236D}$ and $Sec14^{R65A,T236W}$, and these Sec14s were anticipated to exhibit specific PtdIns-binding defects superior to those of the characterized $Sec14^{K66A,K239A}$ (Phillips et al., 1999).

Finally, $Sfh1^{S175I,T177I}$ was engineered for specific ablation of PtdCho binding by substitution of S175 and T177 (residues that coordinate the PtdCho headgroup phosphate)

with Ile (Figure S3C; Sec14 cognate is Sec14^{S173I,T175I}). These alterations should sterically hinder incorporation of amino-PL head-group phosphate into the Sfh1 cavity. ESI-mass spectrometry reports that, in contrast to Sfh1 (which binds PtdEtn when expressed in *E. coli*), Sfh1^{S175I,T177I} loads with phosphatidylglycerol (PtdGro) (Figure S4). The data suggest Sfh1^{S175I,T177I} loads with PtdGro in its PtdIns-binding site because it cannot load with amino-PLs. By contrast, a recombinant Sfh1^{S175A,T177A} purifies in a PtdEtn-loaded form (Figure S4; Sec14 cognate is Sec14^{S173A,T175A}).

PL-Transfer Activities of Mutant Sec14 Derivatives

The mutant Sec14 derivatives exhibited the expected signature defects in PL-transfer activity. PL transfer assays were initially conducted with cytosol prepared from derivatives of a *sec14Δ cki1* yeast strain that individually express each mutant Sec14 to high levels. The parental *sec14Δ cki1* mutant is viable in absence of the normally essential Sec14, and cytosol prepared from that strain harbors no measurable PtdIns- or PtdCho-transfer activity (Phillips et al., 1999; Li et al., 2000). All Sec14 derivatives were expressed to equivalent levels in vivo and were stable under conditions of the assay (Figure 4A). Sec14-containing cytosol exhibited robust PtdIns- and PtdCho-transfer activities, Sec14^{M177W,V194W} cytosol harbored no measurable PtdIns- or PtdCho-transferactivity,and Sec14^{S173A,T175A}and Sec14^{S173I,T175I} cytosols each manifested PtdIns-transfer activity. The latter cytosol exhibited no PtdCho-transfer activity, whereas Sec14^{R65A,T236D} and Sec14^{R65A,T236W} cytosol were extinguished for PtdIns-transfer activity only (Figure 4B).

These biochemical properties were recapitulated with recombinant Sec14, Sec14^{M177W,V194W}, Sec14^{S173I,T175I}, Sec14^{S173A,T175A}, Sec14^{R65A,T236D}, and Sec14^{R65A,T236W} (Figure 4C). The Sec14^{M177W,V194W} pinch mutant presented no measurable PtdCho-transfer activity, although trace PtdIns-transfer activity was measured at high-protein concentrations (Figure 4C). Titration experiments indicate Sec14^{M177W,V194W}-specific activity for PtdIns and PtdCho transfer is reduced 125-fold and ≥300-fold relative to Sec14, respectively. With regard to mutant Sec14 derivatives with headgroup-specific defects, Sec14^{S173A,T175A} and Sec14^{S173I,T175I} both retained wild-type PtdIns-transfer activity, although no PtdCho-transfer activity was measured for Sec14^{S173I,T175I} (Figure 4C). We estimate Sec14^{S173I,T175I}-specific activity for PtdCho transfer is reduced ≥300-fold relative to Sec14. Finally, Sec14^{R65A,T236D} and Sec14^{R65A,T236W} retained PtdCho-transfer activity, but specific activities for PtdIns transfer are reduced ≥300-fold relative to Sec14 (Figure 4C). As expected, these two mutants were more defective for PtdIns transfer than the previously characterized PtdIns binding-defective Sec14^{K66A,239A} (Figure 4C).

PtdCho and PtdIns Binding Are Both Required for Essential Sec14 In Vivo Functions

Genetic complementation tests assessed functionality of Sec14^{M177W,V194W}, Sec14^{S173A,T175A}, Sec14^{S173I,T175I}, Sec14^{R65A,T236D}, and Sec14^{R65A,T236W}. Mutant proteins were expressed from the *SEC14* promoter, and functionality was interrogated in three ways: (1) complementation of the hypomorphic *sec14–1^{ts}* mutation, (2) complementation of *sec14–1^{ts}* in a mutant strain defective in phospholipase D (PLD) activity —a defect that enhances *sec14–1^{ts}* phenotypes), and (3) plasmid shuffle assays that discern whether a mutant Sec14 fulfills essential Sec14 functions in vivo. The Sec14^{M177W,V194W}

pinch mutant was uniformly defective in all three functional assays (Figure 5A). Analyses of a more extensive set of Sec14 pinch mutants reinforce these results. First, inability of Sec14^{V194W} expression to complement *sec14* mutations (while Sec14^{M177W} retained some activity in these assays) suggests this substitution is primarily responsible for steric obstruction of acyl chain space (Figure S5A). Second, Sec14^{A197W} and Sec14^{M177W,A197W} also score as defective in all complementation assays tested (Figure S5A). The intracellular steady-state levels of pinch-close mutants were comparable to those of native Sec14 under all complementation assay conditions (Figure 5B).

Functional complementation tests also identified the PtdCho-binding-defective Sec14^{S173I,T175I} as a defective polypeptide. Sec14^{S173I,T175I} expression failed to rescue *sec14–1^{ts}* growth defects, although some growth is recorded if cells are incubated for >96 hr. No rescue was scored when Sec14^{S173I,T175I} was expressed in PLD-deficient *sec14–1^{ts} spo14Δ* mutants (Figure 5A), and Sec14^{S173I,T175I} failed to execute essential Sec14 functions as determined by lack of plasmid shuffle. Inability of Sec14^{S173I,T175I} to rescue *sec14Δ*-associated lethality was apparent even when gene dosage of the *sec14^{S173I,T175I}* allele was increased (Figure 5A). Sec14^{S173I,T175I} accumulated to physiological levels under conditions of the complementation tests at 30°C (Figure 5B) and 37°C (data not shown). Additional mutagenesis experiments indicated only the PtdCho-binding-deficient Sec14^{S173I,T175I} and Sec14^{T175W} were functionally inactive (Figure S5A).

Finally, Sec14^{R65A,T236D} and Sec14^{R65A,T236W} phenotypic data report expression of PtdIns binding/exchange-deficient proteins fails to rescue *sec14–1^{ts}*-associated growth defects or to restore viability to *sec14Δ* yeast mutants, as indicated by plasmid shuffle (Figure 5A). Conclusions regarding inability of these proteins to complement *sec14–1^{ts}* are softened by reduced stability of both when yeast are cultured for extended periods at 37°C, but Sec14^{R65A,T236D} and Sec14^{R65A,T236W} are stable under the 30°C conditions of the plasmid shuffle assay (Figure 5B). All other mutants generated with the goal of specifically compromising PtdIns binding proved leakier and scored as functional in vivo so long as protein stability was maintained (Figure S5A). Thus, PtdIns binding is also an essential Sec14 activity. All biologically defective Sec14s shared an independent property, i.e., yeast expressing these proteins as sole sources of Sec14 function exhibited PLD activities elevated in proportion to magnitude of the Sec14 defect (Figure S5B).

Mutant Sec14s and Golgi Secretory Function

Phenotypic rescue by mutant Sec14 expression was accompanied by correction of trafficking defects associated with Sec14 insufficiencies. Robust secretion of invertase was restored by Sec14 and Sec14^{S173A,T175A} expression relative to the *sec14–1^{ts}* negative control (Figure 5C). By contrast, neither expression of Sec14^{M177W,V194W}, Sec14^{S173I,T175I}, Sec14^{R65A,T236D}, nor Sec14^{R65A,T236W} improved invertase transport in *sec14–1^{ts}* yeast. These mutant *sec14* proteins were stable under conditions of these experiments (Figure 5B). Pulse-chase radiolabeling analyses that monitored carboxypeptidase Y (CPY) transit through the yeast secretory pathway to the vacuole yielded similar conclusions. Core glycosylated p1 CPY (67 kDa; diagnoses ER and early Golgi pools) is serially converted to the terminally glycosylated p2 TGN form and, finally, the mature mCPY (61 KDa) upon delivery to the

vacuole (Stevens et al., 1982; Ammerer et al., 1986). Sec14^{S173A,T175A} expression supported efficient CPY transport in *sec14–1*^{ts} mutants at 37°C (Figure 5D). Sec14^{M177W,V194W}, Sec14^{S173I,T175I}, Sec14^{R65A,T236D}, or Sec14^{R65A,T236W} expression failed to restore efficient CPY transport to the vacuole (Figure 5D). Although neither Sec14^{R65A,T236D} nor Sec14^{R65A,T236W} expression afforded any rescue of CPY trafficking defects, modest improvements in CPY delivery to the vacuole were supported by Sec14^{S173I,T175I} expression (Figure 5D). Morphological confirmation of the invertase and CPY data was obtained from electron microscopic analyses (Figures S6A and S6B).

Sec14 PL-Binding Activities Must Reside In *cis*

With regard to the headgroup-specific PL-binding mutants Sec14^{S173I,T175I} and Sec14^{R65A,T236D}, no obvious defects in intracellular localization pattern were noted relative to Sec14 (data not shown)—suggesting a fundamental defect in Sec14 activity. The functional requirement for both PtdIns- and PtdCh-binding activities raised the question of whether these must be housed ,in *cis*- (i.e., in the same molecule) or whether a mixed population of Sec14::PtdIns and Sec14::PtdCho molecules satisfies the essential Sec14 requirement for cell viability. Plasmid shuffle assays were used to interrogate these possibilities (see Supplemental Experimental Procedures). Both YCp(*myc-sec14*^{S173I,T175I}) and YCp(*myc-sec14*^{R65A,T236D}) plasmids were introduced into the *sec14Δ* YEp(*SEC14*) shuffle strain, and transformants carrying all three plasmids were incubated under conditions where nutritional selection for YEp(*SEC14*) was relieved. No YEp(*SEC14*) loss was detected when both YCp(*myc-sec14*^{S173I,T175I}) and YCp(*myc-sec14*^{R65A,T236D}) were present (Figure 5E). YEp(*SEC14*) loss was not hampered by the requirement of inheriting two plasmids, as robust shuffling of plasmids was scored in cells carrying YCp(*myc-sec14*) and the YCp vector control under selection for both plasmids (Figure 5E). cDNA sequence analyses confirmed expression of both mutant *myc*-tagged *sec14* genes (Figure 5F), and transformants carrying either of the *myc-sec14* constructs with the second selection marker expressed stable protein (Figure 5G). Thus, PtdIns- and PtdCho-binding activities must be configured in *cis* to reconstitute a functional Sec14.

Potentiation of PIP Homeostasis by Mutant *sec14* Proteins In Vivo

The abilities of Sec14^{S173I,T175I} and Sec14^{R65A,T236W} to regulate PIP metabolism in vivo were quantified. Each protein was expressed in a *sec14Δ cki1* yeast strain (CTY303; see Supplemental Experimental Procedures). This ,bypass Sec14- strain exhibits basal PIP levels, due to its Sec14 deficiency, and provides a context for assessing ability of a protein to modulate PIP metabolism (Phillips et al., 1999; Routt et al., 2005). The major glycerophospho-Ins species (PtdIns, PtdIns 3-phosphate [PtdIns-3-P], PtdIns 4-phosphate [PtdIns-4-P], and PtdIns 4,5-bisphosphate [PtdIns-4,5-P_2]) are apparent in *SEC14* strains (Figure 6A). By contrast, the *sec14Δ cki1* control exhibited ~2-fold reductions in bulk PtdIns-3-P, PtdIns-4-P, and PtdIns-4,5-P_2. Expression of the PtdIns-binding-defective Sec14^{R65A,T236D} failed to restore wild-type PIP profiles to the *sec14Δ cki1* strain (Figure 6A). In accord with the complementation data, Sec14^{S173I,T175I} also failed to rescue PIP levels in the *sec14Δ cki1* strain; even in the face of its robust in vitro PtdIns-transfer activity.

To assess Sec14-mediated activation of a yeast PtdIns 4-OH kinase in its native environment, we exploited the selective Sac1 PIP phosphatase-mediated degradation of the PtdIns-4-P generated by the Stt4 PtdIns 4-OH kinase (Nemoto et al., 2000; Foti et al., 2001). The 10-fold accumulation of PtdIns-4-P in Sac1-deficient yeast reports Stt4 activity. Again, the dynamic range of PtdIns-4-P accumulation in Sec14-proficient versus -deficient *sac1* mutants was 2-fold. Neither $Sec14^{S173I,T175I}$ nor $Sec14^{R65A,T236D}$ rescued the depressed Stt4 activity of Sec14-deficient *sac1* yeast (Figure 6B). Thus, $Sec14^{S173I,T175I}$ and $Sec14^{R65A,T236D}$ both fail to potentiate Stt4-dependent PtdIns-4-P synthesis in vivo.

In Situ Phosphorylation of PtdIns in a Soluble Sec14::PtdIns Complex

We attempted to dissect Sec14 potentiation of PtdIns kinase activity in a defined in vitro system by exploiting Sec14 promiscuity in stimulation of heterologous PtdIns kinases (Hübner et al., 1998; Jones et al., 1998; Phillips et al., 1999). Mammalian Pik1 (PtdIns 4-OH kinase IIIβ) was used as model kinase. The assays employed PtdIns incorporated into authentic liposomes. Sec14 evoked a time and protein-dependent stimulation in PtdIns-4-P production under conditions where liposomal PtdIns substrate was not limiting (10 mol% PL; Figure 6C). The PtdIns-binding mutant $Sec14^{R65A,T236D}$ elicited no effect, indicating stimulation required PtdIns binding by Sec14. In contrast to the in vivo results, the PtdCho-binding mutant $Sec14^{S173I,T175I}$ also stimulated the kinase (Figure 6C).

Two lines of evidence indicate the Sec14-dependent in vitro phosphorylation reaction is not of physiological relevance. First, it is inefficient. Only 0.02 PtdIns-4-P was produced per Sec14 (or $Sec14^{S173I,T175I}$)—a stoichiometry that suggests Sec14-mediated kinase stimulation reports in situ phosphorylation of Sec14-bound PtdIns. Indeed, PtdIns bound to either Sec14 or $Sec14^{S173I,T175I}$ is accessible (poorly) to PtdIns kinase in vesicle-free reactions where the PtdIns-binding-defective $Sec14^{R65A,T236D}$ is again silent (Figure 6D). The poor access of PtdIns kinase to Sec14-bound substrate likely reflects sequestration of the PtdIns headgroup in the soluble Sec14::PtdIns (Figure S2). Second, in situ phosphorylation of Sec14-bound PtdIns forms a dead-end Sec14::PtdIns-4-P complex. Sec14 cannot release bound PtdIns-4-P into acceptor membranes (%5% of Sec14::PtdIns-4-P complexes unload bound PIP). Finally, Sec14 cannot extract PtdIns-4-P from membranes, nor can Sec14 transfer PtdIns-4-P in vitro.

Sec14-Mediated Regulation of PIP Synthesis Counters the Action of Kes1

Sec14 bolsters PtdIns kinase activity in vivo to counter the antagonistic effects levied by the Kes1 oxysterol-binding protein on Pik1 PtdIns 4-OH kinase action. Pik1 maintains a Golgi PtdIns-4-P pool required for efficient membrane trafficking from the TGN (Hama et al., 1999; Walch-Solimena and Novick, 1999; Strahl et al., 2005). Kes1 deficiencies elicit both ,bypass Sec14- and partial rescue of $pik1^{ts}$ alleles, suggesting Kes1 antagonizes the Sec14 pathway as a Pik1 inhibitor (Fang et al., 1996; Li et al., 2002). Indeed, Kes1 defects substantially rescue the PtdIns-4-P deficits of Sec14-deficient yeast, and this rescue of PtdIns-4-P mutants is not compromised by loss of PLD (Figure 6E)—even though PLD activity is essential for *kes1*-mediated bypass Sec14 (Xie et al., 1998).

DISCUSSION

Elucidation of mechanisms for how Sec14-like proteins regulate membrane trafficking requires detailed description of how such proteins translate PL binding to biological function. These issues are clarified herein. We report high-resolution crystal structures of the yeast Sec14 homolog Sfh1 in complex with biologically relevant PLs, and these Sfh1 structures are translated to detailed functional analyses of Sec14. Five conclusions derive from these analyses: (1) Sfh1/Sec14 bind PtdCho and PtdIns differentially, (2) PtdCho- and PtdIns-binding activity are each required for Sec14 to fulfill its essential in vivo roles, (3) Sec14 must house both PtdIns- and PtdCho-binding in *cis* for biological activity, (4) PtdIns and PtdCho binding are both required for Sec14-mediated regulation of PIP homeostasis, and (5) Sec14-mediated potentiation of PIP homeostasis counters the action of the Kes1 oxysterol-binding protein that antagonizes Pik1 PtdIns 4-OH kinase action. Demonstration that exchange of two disparate ligands is required for Sec14-mediated stimulation of PIP synthesis suggests a strategy through which members of the Sec14 superfamily may coordinate diverse signals with PIP metabolism, and thereby couple PIP metabolism to highly specific physiological responses. The data also reveal the involvement of ubiquitous, yet poorly understood, proteins in regulating pathways that antagonize the action of PtdIns kinases in vivo.

Structural Insights into the Mechanics of Sec14-like Proteins

All holo-Sfh1 structures describe ,closed- conformers where the A9/T3 hybrid helix lies adjacent to helix A8 and sequesters the PL-binding pocket from solvent. This configuration confirms in silico simulations for how the Sec14 hydrophobic pocket is gated (Ryan et al., 2007). It is also consistent with structural features of closed forms of other Sec14-like proteins (Stocker et al., 2002; Meier et al., 2003; Min et al., 2003; Welti et al., 2007). Comparisons of Sfh1::PtdCho and Sfh1::PtdIns structures indicate minimal conformational adjustment is required for Sfh1 to bind PtdCho versus PtdIns. In that regard, five ordered H_2O molecules fill the unoccupied position of the phospho-Ins group in Sfh1::PtdCho, and two ordered H_2O occupy the site vacated by phospho-Cho in Sfh1::PtdIns. Relative binding energies can be calculated from K_Ds ($\Delta\Delta G$). Given Sec14 exhibits a 16-fold preference for PtdIns versus PtdCho (Daum and Paltauf, 1984), we calculate a difference of 1.71 kcal/mol —i.e., Sec14 selectivity for PtdIns versus PtdCho corresponds to release of 0.5 H_2O. As three ordered H_2O are released from the Sfh1 PL pocket during PtdCho/PtdIns exchange, H_2O flux balances the differences in relative binding energies. The excess-free energy released may also offset entropic penalties associated with establishment of the intricate network that engages the PtdIns headgroup.

Biochemical Mechanisms for Sec14 Function in Regulating PIP Homeostasis

PL-transfer and sensor models describe potential mechanisms for Sec14 function (Ile et al., 2006). Both models consider soluble Sec14::PL forms as functional intermediates. In the former case, these are active vehicles for PtdIns delivery. In the latter, these hold intrinsic regulatory power. A third possibility is described by presentation mechanisms where Sec14 stabilizes PtdIns in a configuration where it is a superior substrate for PtdIns kinases. Our data indicate all of these simple models are inadequate. Existence of bypass Sec14 mutants

that diminish PtdCho bio-synthetic capacity, in conjunction with demonstrations that yeast mutants whose most abundant PL is PtdIns still require Sec14 for viability, argues against PL transfer (Cleves et al., 1991b). Strict Sec14 sensor models are inconsistent with demonstrations that coexpression of restricted Sec14::PtdIns and Sec14::PtdCho forms fails to reconstitute Sec14 function in vivo.

Simple PtdIns presentation models also fail. Given PtdIns abundance in yeast (Carman and Zeimetz, 1996), and Sec14 preference for PtdIns versus PtdCho (Daum and Paltauf, 1984), a cycle of PtdIns-binding/modification should operate efficiently in a PtdCho-independent manner. We find in situ phosphorylation of PtdIns in a soluble Sec14::PtdIns complex is a biologically untenable mechanism of Sec14-mediated potentiation of PtdIns kinases. That reaction is inefficient because of steric occlusion of the Ins headgroup, and its successful execution inactivates the host Sec14 molecule as bound PtdIns-4-P cannot be released—presumably because the 4-OH phosphate further stabilizes Sec14::PL interactions. Therefore, any mechanistic description of Sec14 action must either minimize potential for PtdIns-4-P incorporation into the binding pocket or invoke existence of a release factor that stimulates PtdIns-4-P discharge from Sec14.

The requirement that both PtdIns and PtdCho binding must reside in *cis* to potentiate Sec14-mediated PtdIns-kinase action argues that these activities operate in a concerted fashion and suggests how Sec14 may activate PtdIns kinases. We propose heterotypic PtdIns/PtdCho exchange reactions uniquely prime Sec14 for productive presentation of PtdIns to PtdIns kinases at the membrane surface (Figure 7). This hypothesis is attractive on several grounds. It describes a mechanism for (1) solving the kinase/membrane PtdIns accessibility problem, (2) how a productive and PtdCho-dependent interfacial presentation reaction occurs, (3) why Sec14 binds PtdIns and PtdCho at different sites, and (4) how the reaction ensures PtdIns-4-P will not invade the Sec14 pocket. In heterotypic reactions that exchange bound PtdIns for PtdCho, an invading PtdCho forces PtdIns from the pocket—thereby generating a kinase-susceptible PtdIns intermediate. In this scenario, PtdCho-entry and PtdIns-exit portals are distinct, there is no apo-Sec14 intermediate during PL-exchange, and surface proximity of the PtdIns headgroup facilitates formation of the kinase-susceptible intermediate (Figure 7A).

A second, and not mutually exclusive, alternative suggests a reciprocal mechanism. Because the PtdIns headgroup binding site lies near the Sec14 surface, and bound PtdCho is buried, a kinetic mismatch is generated when Sec14 unloads a deeply sequestered PtdCho (slow exit) from its pocket in favor of PtdIns (fast entry). This asymmetry ensures the invading PtdIns is delayed in a partially incorporated state where it is susceptible to kinase attack (Figure 7B). Completion of PtdCho unloading clears the pocket, and apo-Sec14 reloads with PL. In this scenario, PtdIns-entry and PtdCho-exit portals overlap (Figure 7B). In both priming models, homotypic PtdCho exchanges are clearly silent, whereas priming does not occur efficiently in homotypic PtdIns exchange.

Biological Rationale for Sec14-Mediated Regulation of PtdIns Kinases

We propose that heterotypic Sec14 PL exchange serves as an iterative engine for rendering PtdIns monomers as superior kinase substrates. Why is this biologically necessary? The data

indicate Sec14-mediated activation of the Pik1 PtdIns 4-OH kinase is an essential activity that counteracts the effect of Kes1 in antagonizing Pik1 action. This point is evidenced by the fact that Kes1 loss-of-function effects both bypass Sec14 and partial rescue of *pik1^{ts}* mutations (Fang et al., 1996; Li et al., 2002) and by our demonstration that Kes1 inactivation rescues PtdIns-4-P levels in Sec14-deficient mutants. Kes1 may inhibit Pik1 directly, stimulate PtdIns-4-P degradation, or exert these effects indirectly through other homeostatic mechanisms (e.g., sterols). As Kes1 binds both PIPs and sterols (Li et al., 2002; Im et al., 2005), all three scenarios remain viable.

KES1 was first identified via *kre11* suppressor mutations in cell wall biosynthesis (Al-Aidroos and Bussey, 1978). Kre11 is one of three dispensable subunits of the TRAPP complex that promotes Ypt31/32 Rab-dependent trafficking from the TGN (Sacher et al., 2001). That *kes1* mutations effect bypass Sec14, influence Pik1-dependent PtdIns-4-P pools, and bypass Kre11, when coupled with our observations that TRAPP subunit (*trs85* and *kre11*) and Ypt Rab GTPase activating protein (*gyp1*) mutations exhibit synthetic genetic interactions with *sec14–1^{ts}* (Table S1) and *pik1^{ts}* alleles (Sciorra et al., 2005), is consistent with Sec14 and Pik1 potentiating Ypt31/32-dependent trafficking from the TGN (as depicted in Figure 7). Alternatively, *kes1* alleles may activate parallel TGN export pathways. Indeed, inactivation of ARF-dependent membrane trafficking also elicits synthetic effects when combined with *sec14–1^{ts}* (Table S1)—suggesting Sec14 regulates multiple TGN export pathways. Several lines of evidence support this idea. First, bypass Sec14 mutations that inactivate PtdCho biosynthesis do not rescue PtdIns-4-P levels and do not rescue *pik1^{ts}* (Phillips et al., 1999; Li et al., 2002). Second, PLD is required for bypass Sec14 irrespective of PtdIns-4-P status. Third, Sec14 defects strongly block invertase secretion (Bankaitis et al., 1989), whereas Pik1 defects exert modest effects (Walch-Solimena and Novick, 1999). Finally, Bgl2 trafficking, which involves vesicles distinct from those that ferry invertase (Harsay and Bretscher, 1995), is strongly affected by *pik1^{ts}* but is less affected by *sec14–1^{ts}*. Thus, bypass Sec14 mutations may promote cargo resorting between TGN export pathways.

Functional Implications for the Sec14-Protein Superfamily

A requirement for PtdCho-dependent priming for Sec14-mediated PtdIns-kinase stimulation suggests diverse lipophiles could similarly prime other Sec14-like proteins for PtdIns/PIP presentation to modifying enzymes. Such a priming circuitry offers interesting coincidence-detection mechanisms for imposing precise control onto specific PIP pools in response to specific physiological signals. In that regard, yeast Sec14-like (*SFH*) proteins devoid of PtdCho-transfer activity provide interesting cases (Li et al., 2000). These *SFH* proteins bind both PtdIns and PtdEtn (a priming ligand?). PtdIns-binding motifs are also obvious in Sec14-like proteins that bind lipophiles (e.g., α-tocopherol) but are not presently known to bind PLs (Figure S7). We speculate such Sec14-like proteins may exhibit as yet unrecognized PIP signaling capabilities. When coupled with the evolutionary expansion of the Sec14 superfamily, the two-ligand priming mechanism suggests an expansive scale and intricacy for the regulatory interfaces between Sec14 proteins and the metabolic control/signal transduction landscape of eukaryotic cells.

EXPERIMENTAL PROCEDURES

Reagents

Standard reagents were purchased from Sigma (St. Louis, MO) or Fisher (Norcross, GA), and all PLs were purchased from Avanti (Alabaster, AL). Descriptions of yeast strains, genetic methods, and purification of various PL-bound forms of recombinant Sfh1 purification are detailed in the Supplemental Experimental Procedures.

Crystallization and Structure Determination

Sfh1::PtdEtn crystals were grown by sitting drop vapor diffusion at 22°C from solutions containing 1.5 μl of protein at ~5.25 mg/mL protein and 1.5 μl of crystallant: 25.5% (w/v) PEG 4000, 15% (w/v) glycerol and 170 mM potassium acetate, 85 mM Tris (pH 8.5). Crystals were grown in cryoprotectant and flash-cooled in liquid N_2. Data to 1.9 Å resolution were collected at 100 K at the South East Regional Collaborative Access Team (SER-CAT) beamline at Argonne National Labs and processed and scaled with HKL2000 (Table S1) (Otwinowski, 1993). Initial phases were determined using the Sec14 structure as a molecular replacement search model (Sha et al., 1998). Model building and refinement were performed using standard methods in Coot (Emsley and Cowtan, 2004) and CNS (Brünger et al., 1998), respectively. The final model contains one Sfh1 monomer (residues 4–310) and one bound PtdEtn in the asymmetric unit.

Crystals of Sfh1::PtdIns and Sfh1::PtdCho complex were grown by hanging drop vapor diffusion at 22°C from solutions containing 0.8 μl of protein at ~5 mg/mL and 1.2 μl of the following crystallant: 15%–25% PEG 3350, 5% glycerol, and either 100 mM ammonium sulfate or 100 mM potassium phosphate, 100 mM ammonium acetate (pH 4.6). Crystals were cryoprotected in 30% PEG 3350, 30% glycerol, and 200 mM ammonium sulfate, 100 mM ammonium acetate (pH 4.6). Data to 1.86 Å resolution for the Sfh1::PtdIns complex were collected at SER-CAT at Argonne National Labs, whereas data to 2.0 Å resolution for the Sfh1::PtdCho complex were collected at the Stanford Synchrotron Radiation Laboratory (SSRL) beamline 11–1. All data were processed and scaled with HKL2000 (Table 1) (Otwinowski, 1993). Initial phases were determined by using the Sfh1::PtdEtn structure as a molecular replacement search model. Final models for Sfh1::PtdIns and Sfh1::PtdCho contain one (residues 4–310) and two (residues 4–310) monomers per asymmetric unit, respectively. His_8-Sfh1 was also incubated with vesicles containing a PtdCho and PtdIns mixture (60:40 mol%). The Sfh1::PL complex was crystallized, and data to 2.03 Å were collected and processed as described for the Sfh1::PtdEtn complex. Both PtdCho and PtdIns were subsequently modeled in the electron density, and occupancies were refined in CNS (Brünger et al., 1998).

Lipid Extraction and Mass Spectrometry

Lipids were extracted from Sfh1 crystals with a single-phase $CHCl_3$/methanol/H_2O system (1:2:0.8) and analyzed in negative-ion, multichannel acquisition mode (Schaaf et al., 2006). CID-MS was performed as described (Schaaf et al., 2006).

Lipid Kinase Assays

Assays were performed as described (Downing et al., 1996). Standard reactions (final volume 60 μL) contained 300 mM NaCl, 40 mM Tris (pH 7.5), 25 mM $MgCl_2$, 10 mM Na-phosphate (pH 7.5), 1 mM EGTA, 0.1 mM (1 μCi) [$\gamma-^{32}$P] ATP, and 2.5 μg of GST-tagged PtdIns 4-OH kinase IIIβ purified as described (Zhao et al., 2000) with minor modification. Reactions contained unilamellar PtdIns (10%)/PtdCho (90 mol %) liposomes (total lipid concentration in the assay was 1.4 mM), and recombinant Sec14 proteins were titrated. Liposomes were generated by extrusion (0.8 μm pore size polycarbonate filter) using a hand extruder (Avanti). Reactions were initiated by addition of [$\gamma-^{32}$P] ATP, incubated at 30°C (15 min), terminated, and PtdIns-4-P extracted as described (Downing et al., 1996). To determine optimal PtdIns-4-P production under any given condition, 0.4% Triton X-100 was added to the standard reaction. PtdIns-4-P identity was confirmed by thin layer chromatography using PtdIns-4-P standards.

Supplementary Material

Refer to Web version on PubMed Central for supplementary material.

ACKNOWLEDGMENTS

We thank Laurie Betts (UNC) for technical advice, Tamas Balla (NIH) for providing the PtdIns 4-OH kinase IIIβ plasmid, Guendalina Rossi and Hao Wu (UNC) for help with Bgl2 assays, and John York (Duke) for help with PIP analyses. This work was supported by NIH grant GM44530 to V.A.B. G.S. is a postdoctoral fellow of the Deutsche Forschungsgemeinschaft (SCHA 1274/1-1) and K.R.T. is a postdoctoral trainee of the NIH Molecular Mycology and Pathogenesis Training Grant (5T32-AI052080). E.A.O. and M.R.R. were supported by NIH grant DK62229. E.A.O. was also supported by a Lineberger Comprehensive Cancer Center Postdoctoral Fellowship. T.A.G. and C.R.H.R. were supported by the NIH LIPID MAPS Large Scale Collaborative Grant (GM069338). We acknowledge the UNC Lineberger Comprehensive Cancer Center Genome Analysis and Nucleic Acids Core facilities. Please contact E.A.O. for crystallography data (eric.ortlund@emory.edu).

REFERENCES

Al-Aidroos K, and Bussey H (1978). Chromosomal mutants of *Saccharomyces cerevisiae* affecting the cell wall binding site for killer factor. Can. J. Microbiol 24, 228–237. [PubMed: 348280]

Ammerer G, Hunter CP, Rothman JH, Saari GC, Valls LA, and Stevens TH (1986). *PEP4* gene of *Saccharomyces cerevisiae* encodes proteinase A, a vacuolar enzyme required for processing of vacuolar precursors. Mol. Cell. Biol 6, 2490–2499. [PubMed: 3023936]

Aravind L, and Koonin EV (1999). Gleaning non-trivial structural, functional and evolutionary information about proteins by iterative database searches.J. Mol. Biol 287, 1023–1040. [PubMed: 10222208]

Bankaitis VA, Malehorn DE, Emr SD, and Greene R (1989). The *Saccharomyces cerevisiae SEC14* gene encodes a cytosolic factor that is required for transport of secretory proteins from the yeast Golgi complex. J. Cell Biol 108, 1271–1281. [PubMed: 2466847]

Bankaitis VA, Aitken JR, Cleves AE, and Dowhan W (1990). An essential role for a PL transfer protein in yeast Golgi function. Nature 347, 561–562. [PubMed: 2215682]

Benomar M, Yahyaoui F, Meggouh A, Bouhouche M, Boutchich N, Bouslam N, Zaim A, Schmitt M, Belaidi H, Ouazzani R, et al. (2002). Clinical comparison between AVED patients with 744 del A mutation and Friedreich ataxia with GAA expansion in 15 Moroccan families. J. Neurol. Sci 198, 25–29. [PubMed: 12039660]

Bomar JM, Benke PJ, Slattery EL, Puttagunta R, Taylor LP, Seong E, Nystuen A, Chen W, Albin RL, Patel PD, et al. (2003). Mutations in a novel gene encoding a CRAL-TRIO domain cause human

Cayman ataxia and ataxia/ dystonia in the jittery mouse. Nat. Genet 35, 264–269. [PubMed: 14556008]

Brünger AT, Adams PD, Clore GM, DeLano WL, Gros P, Grosse-Kunstleve RW, Jiang J-S, Kuszewski J, Nilges M, Pannu NS, et al. (1998). Crystallography and NMR system: a new software suite for macromolecular structure determination. Acta Crystallogr. D Biol. Crystallogr 54, 905–921. [PubMed: 9757107]

Carman GM, and Zeimetz GM (1996). Regulation of PL biosynthesis in the yeast Saccharomyces cerevisiae. J. Biol. Chem 271, 13292–13296. [PubMed: 8663093]

Cleves AE, McGee TP, and Bankaitis VA (1991a). PL transfer proteins: a biological debut. Trends Cell Biol 1, 30–34. [PubMed: 14731807]

Cleves AE, McGee TP, Whitters EA, Champion KM, Aitken JR, Dowhan W, Goebl M, and Bankaitis VA (1991b). Mutations in the CDP-choline pathway for PL biosynthesis bypass the requirement for an essential PL transfer protein. Cell 64, 789–800. [PubMed: 1997207]

D'Angelo I, Welti S, Bonneau F, and Scheffzek K (2006). A novel bipartite PL-binding module in the neurofibromatosis type 1 protein. EMBO Rep. 7, 174–179. [PubMed: 16397625]

Daum G, and Paltauf F (1984). Isolation and partial characterization of a PL transfer protein from yeast cytosol. Biochim. Biophys. Acta 794, 385–391.

Downing GJ, Kim S, Nakanishi S, Catt KJ, and Balla T (1996). Characterization of a soluble adrenal phosphatidylinositol 4-kinase reveals wortmannin sensitivity of type III phosphatidylinositol kinases. Biochemistry 35, 3587–3594. [PubMed: 8639510]

Emsley P, and Cowtan K (2004). Coot: model-building tools for molecular graphics. Acta Crystallogr. D Biol. Crystallogr 60, 2126–2132. [PubMed: 15572765]

Fang M, Kearns BG, Gedvilaite A, Kagiwada S, Kearns M, Fung MKY, and Bankaitis VA (1996). Kes1 shares homology with human oxysterol binding protein and participates in a novel regulatory pathway for yeast Golgi-derived transport vesicle biogensis. EMBO J 15, 6447–6459. [PubMed: 8978672]

Foti M, Audhya A, and Emr SD (2001). Sac1 lipid phosphatase and Stt4 PtdIns-4-kinase regulate a pool of PtdIns(4)P pool that functions in control of the actin cytoskeleton and vacuole morphology. Mol. Biol. Cell 12, 2396–2411. [PubMed: 11514624]

Fruman DA, Meyers RE, and Cantley LC (1998). Phoisphoinositide kinases. Annu. Rev. Biochem 67, 481–507. [PubMed: 9759495]

Hama H, Schnieders EA, Thorner J, Takemoto JY, and DeWald D (1999). Direct involvement of phosphatidylinositol-4-phosphate in secretion in the yeast *Saccharomyces cerevisiae*. J. Biol. Chem 274, 34294–34301. [PubMed: 10567405]

Harsay E, and Bretscher A (1995). Parallel secretory pathways to the cell surface in yeast. J. Cell Biol 131, 297–310. [PubMed: 7593160]

Hübner S, Couvillon AD, Käs JA, Bankaitis VA, Vegners R, Carpenter CL, and Janmey PA (1998). Enhancement of phosphoinositide 3-kinase (PI 3-kinase) activity by membrane curvature and inositol-phospholipid-binding peptides. Eur. J. Biochem 258, 846–853. [PubMed: 9874255]

Ile KE, Schaaf G, and Bankaitis VA (2006). Phosphatidylinositol transfer proteins and cellular nanoreactors for lipid signaling. Nat. Chem. Biol 2, 576–583. [PubMed: 17051233]

Im YJ, Raychaudhuri S, Prinz WA, and Hurley JH (2005). Structural mechanism for sterol sensing and transport by OSBP-related proteins. Nature 437, 154–158. [PubMed: 16136145]

Jones SM, Alb JG Jr., Phillips SE, Bankaitis VA, and Howell KE (1998). A phosphatidylinositol-3-kinase and phosphatidylinositol transfer protein cooperate to drive phosphatidylinositol-3-phosphate-dependent formation of constitutive transport vesicles from the *trans*-Golgi Network. J. Biol. Chem 273, 10349–10354. [PubMed: 9553090]

Li X, Rivas MP, Fang M, Marchena J, Mehrotra B, Chaudhary A, Feng L, Prestwich GD, and Bankaitis VA (2002). Analysis of OSBP homolog Kes1p function in regulation of Sec14p-dependent protein transport from the yeast Golgi complex. J. Cell Biol 157, 63–77. [PubMed: 11916983]

Li X, Routt S, Xie Z, Cui X, Fang M, Kearns MA, Bard M, Kirsch D, and Bankaitis VA (2000). Identification of a novel family of nonclassical yeast PITPs whose function modulates activation of

phospholipase D and Sec14p-independent cell growth. Mol. Biol. Cell 11, 1989–2005. [PubMed: 10848624]

Maiti R, Van Domselaar GH, Zhang H, and Wishart DS (2004) Super-Pose: a simple server for sophisticated structural superposition. Nucleic Acids Res. 32 (Web Server issue), W590–W594. [PubMed: 15215457]

Majerus PW (1997). Inositol phosphatases and kinases in cell signaling. FASEB J. 11, A1297.

Meier R, Tomizaki T, Schulze-Briese C, Baumann U, and Stocker A (2003). The molecular basis of vitamin E retention: structure of human tocopherol transfer protein. J. Mol. Biol 331, 725–734. [PubMed: 12899840]

Min KC, Kovall RA, and Hendrickson WA (2003). Crystal structure of α-tocopherol transfer protein bound to its ligand: Implications for ataxia with vitamin E deficiency. Proc. Natl. Acad. Sci. USA 100, 14713–14718. [PubMed: 14657365]

Nemoto Y, Kearns BG, Wenk MR, Chen H, Mori K, Alb JG Jr., De Camilli P, and Bankaitis VA (2000). Functional characterization of a mammalian Sac1 and mutants exhibiting substrate specific defects in phosphoinositide phosphatase activity. J. Biol. Chem 275, 14446–14456. [PubMed: 10799527]

Otwinowski Z (1993). Data collection and processing In Proceedings of the CCP4 Study Weekend, Sawyer L, Isaacs N, and Bailey S, eds. (Daresbury, UK: SERC Danesbury Laboratory), pp. 56–62.

Ouachi K, Arita M, Kayden H, Faycal H, Hamida MB, Sokol R, Arai H, Inoue K, Mandel J-L, and Koenig M (1995). Ataxia with vitamin E deficiency is caused by mutations in the α-tocopherol transfer protein. Nat. Genet 9, 141–145. [PubMed: 7719340]

Phillips SE, Sha B, Topalof L, Xie Z, Alb JG, Klenchin VA, Swigart P, Cockcroft S, Martin TFJ, Luo M, and Bankaitis VA (1999). Yeast Sec14 deficient in phosphatidylinositol transfer activity is functional in vivo. Mol. Cell 4, 187–197. [PubMed: 10488334]

Phillips SE, Vincent P, Rizzieri K, Schaaf G, Gaucher EA, and Bankaitis VA (2006). The diverse biological functions of phosphatidylinositol transfer proteins in eukaryotes. Crit. Rev. in Bioch. &. Mol. Biol 41, 1–28.

Rivas MP, Kearns BG, Xie Z, Guo S, Sekar MC, Hosaka K, Kagiwada S, York JD, and Bankaitis VA (1999). Relationship between altered phospholipid metabolism, diacylglycerol, ‘bypass Sec14’, and the inositol auxotrophy of yeast *sac1* mutants. Mol. Biol. Cell 10, 2235–2250. [PubMed: 10397762]

Routt SM, Ryan MM, Tyeryar K, Rizzieri K, Roumanie O, Brennwald PJ, and Bankaitis VA (2005). Nonclassical PITPs activate phospholipase D via an Stt4p-dependent pathway and modulate function of late stages of the secretory pathway in vegetative yeast cells. Traffic 6, 1157–1172. [PubMed: 16262726]

Ryan MM, Temple BRS, Phillips SE, and Bankaitis VA (2007). Conformational dynamics of the major yeast phosphatidylinositol transfer protein Sec14: Insights into the mechanisms of PL exchange and diseases of Sec14-like protein deficiencies. Mol. Biol. Cell 18, 1928–1942. [PubMed: 17344474]

Sacher M, Barrowman J, Wang W, Horecka J, Zhang Y, Pypaert M, and Ferro-Novick S (2001). TRAPP I implicated in the specificity of tethering in ER-to-Golgi transport. Mol. Cell 7, 433–442. [PubMed: 11239471]

Schaaf G, Betts L, Garrett TA, Raetz CRH, and Bankaitis VA (2006). Crystallization and preliminary X-ray diffraction analysis of PL-bound Sfh1: A member of the Saccharomyces cerevisiae Sec14-like phosphatidylinositol transfer protein family. Acta Cryst. F 62, 1156–1160.

Sciorra VA, Audhya A, Parsons AB, Segev N, Boone C, and Emr SD (2005). Synthetic gene array analysis of the PtdIns 4-kinase Pik1 identifies components in a Golgi-specific Ypt31/rab-GTPase pathway. Mol. Biol. Cell 15, 2038–2047.

Sha B, Phillips SE, Bankaitis VA, and Luo M (1998). Crystal structure of the Saccharomyces cerevisiae phosphatidylinositol transfer protein Sec14. Nature 391, 506–510. [PubMed: 9461221]

Skinner HB, McGee TP, McMaster CR, Fry MR, Bell RM, and Bankaitis VA (1995). The *Saccharomyces cerevisiae* phosphatidylinositol transfer protein effects a ligand-dependent inhibition of choline-phosphate cytidylyltransferase activity. Proc. Natl. Acad. Sci. USA 92, 112–116. [PubMed: 7816798]

Smirnova T, Chadwick TG, MacArthur R, Poluekov O, Song L, Ryan M, Schaaf G, and Bankaitis VA (2006). The chemistry of PL binding by the Saccharomyces cerevisiae phosphatidylinositol transfer protein Sec14 as determined by electron paramagnetic resonance spectroscopy. J. Biol. Chem 281, 34897–34908. [PubMed: 16997918]

Smirnova T, Chadwick TG, van Tol J, Ozarowski A, Poluektov O, Schaaf G, Ryan MM, and Bankaitis VA (2007). Local polarity and hydrogen bonding inside the Sec14 PL-binding cavity: High-field multifrequency studies. Biophys. J 92, 3686–3695. [PubMed: 17325006]

Stevens TH, Esmon B, and Schekman R (1982). Early stages in the yeast secretory pathway are required for transport of carboxypeptidase Y to the vacuole. Cell 30, 439–448. [PubMed: 6754086]

Stocker A, Tomizaki T, Schulze-Briese C, and Baumann U (2002). Crystal structure of the human supernatant protein factor. Structure 10, 1533–1540. [PubMed: 12429094]

Strahl T, and Thorner J (2007). Synthesis and function of membrane phosphoinositides in budding yeast, *Saccharomyces cerevisiae*. Biochim. Biophys. Acta 1771, 353–404. [PubMed: 17382260]

Strahl T, Hama H, DeWald D, and Thorner J (2005). Yeast phosphatidylinositol 4-kinase, Pik1, has essential roles at the Golgi and in the nucleus. J. Cell Biol 171, 967–979. [PubMed: 16365163]

Vincent P, Chua M, Nogue F, Fairbrother A, Mekheel H, Xu Y, Allen N, Bibikova TN, Gilroy S, and Bankaitis VA (2005). A Sec14p-nodulin domain phosphatidylinositol transfer protein polarizes membrane growth of Arabidopsis thaliana root hairs. J. Cell Biol 168, 801–812. [PubMed: 15728190]

Walch-Solimena C, and Novick P (1999). The yeast phosphatidylinositol-4-OH kinase *PIK1* regulates secretion at the Golgi. Nat. Cell Biol 1, 523–525. [PubMed: 10587649]

Welti S, Fraterman S, D'Angelo I, Wilm M, and Scheffzek K (2007). The sec14 homology module of neurofibromin binds cellular glycerophospholipids: mass spectrometry and structure of a lipid complex. J. Mol. Biol 366, 551–562. [PubMed: 17187824]

Xie Z, Fang M, Rivas MP, Faulkner A, Sternweis PC, Engebrecht J, and Bankaitis VA (1998). Phospholipase D activity is required for suppression of yeast phosphatidylinositol transfer protein defects. Proc. Natl. Acad. Sci. USA 95, 12346–12351. [PubMed: 9770489]

Yanagisawa L, Marchena J, Xie Z, Li X, Poon PP, Singer R, Johnston G, Randazzo PA, and Bankaitis VA (2002). Activity of specific lipid-regulated ARFGAPs is required for Sec14-dependent Golgi secretory function in yeast. Mol. Biol. Cell 13, 2193–2206. [PubMed: 12134061]

Zhao X-H, Bondeva T, and Balla T (2000). Characterization of a recombinant phosphatidylinositol 4-kinase beta reveals auto- and heterophosphorylation of the enzyme. J. Biol. Chem 275, 14642–14648. [PubMed: 10799551]

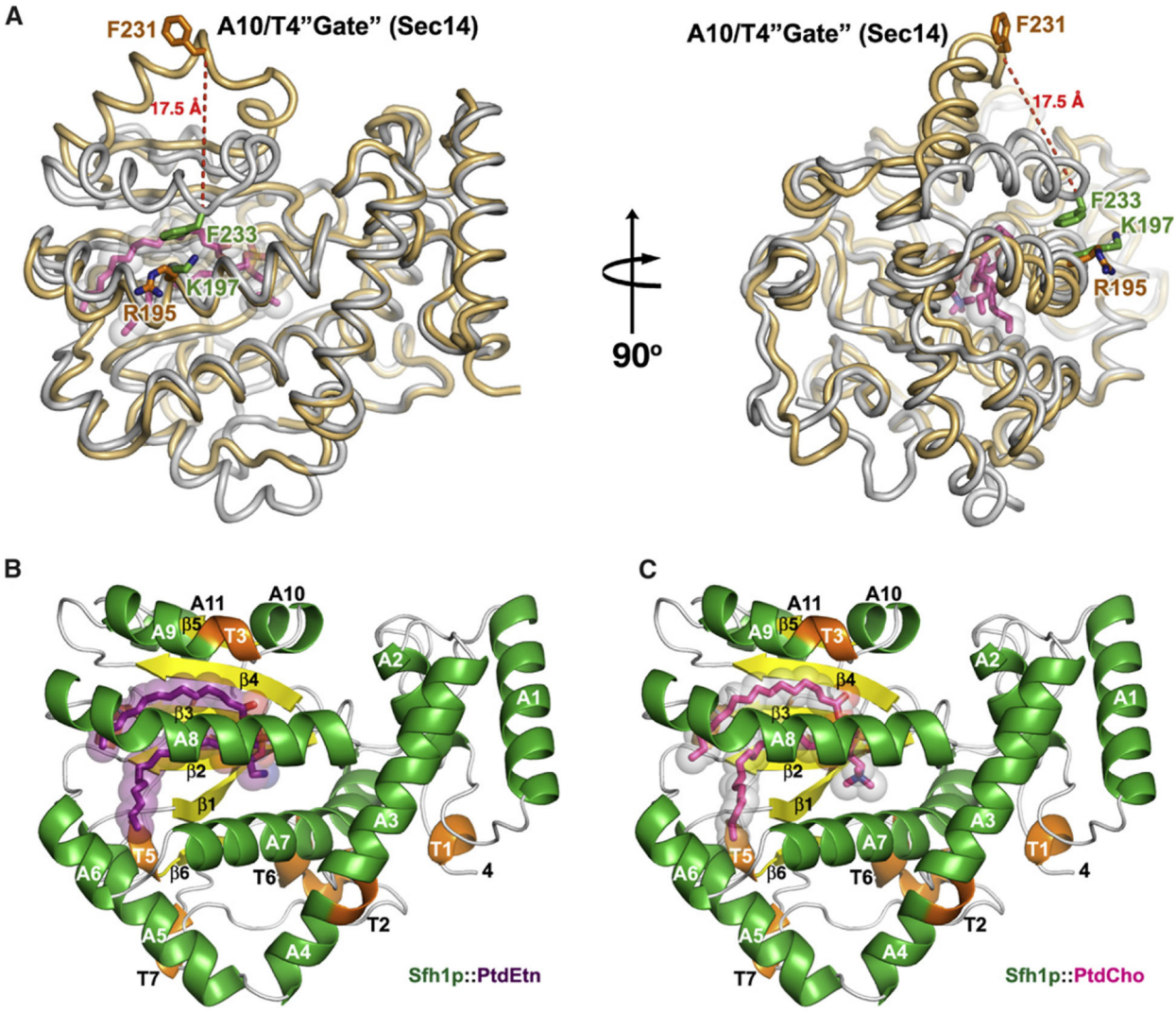

Figure 1. General Properties of a PL-Bound Sfh1 Structure

(A) Superposition of two different orientations of the open Sec14 (light orange) on the Sfh1::PtdEtn complex (gray). The dashed line represents the distance between the α carbons on F231 in Sec14 in the ‚open conformation- and F233 in Sfh1::PtdEtn complex located at the C-terminal end of the A9/T3 helix (A10/T4 helix in Sec14).

(B and C) Ribbon diagram of the Sfh1 component of the Sfh1::PtdEtn complex (α helices in green, 3_{10} helices in orange, and β strands in yellow).

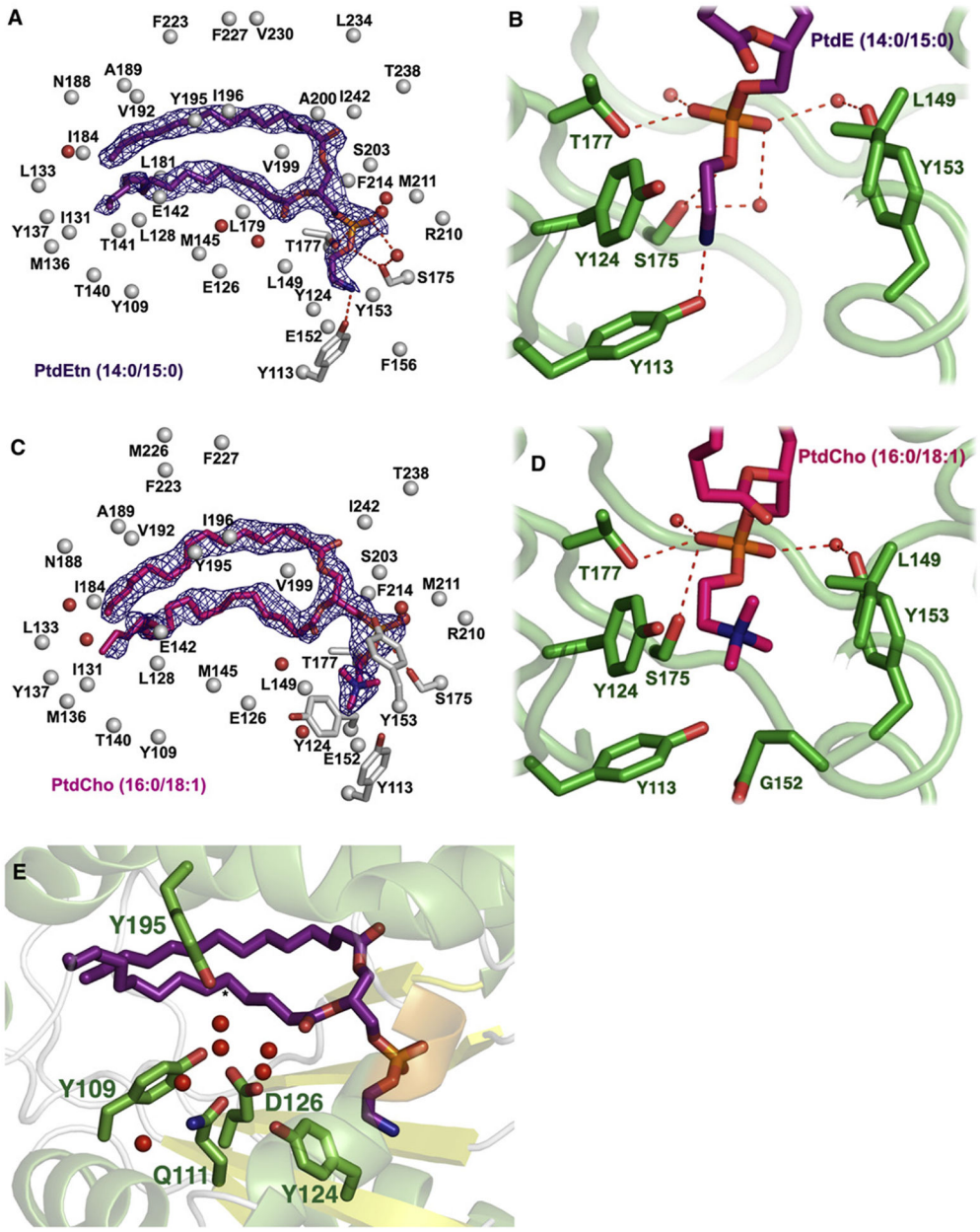

Figure 2. Structures of Sfh1::PtdEtn and Sfh1::PtdCho Complexes

(A–D) $2F_o - F_c$ annealed omit electron density (contoured at 1σ) for the bound PtdEtn (A) and bound PtdCho (C). Residues within 4.2 Å of the bound PLs are shown as white spheres. Residues that coordinate the headgroup moieties are shown as sticks with H bonds represented as dashed lines. (B) PtdEtn and (D) PtdCho headgroup interactions with Sfh1. (E) Depiction of the hydrophilic patch formed by the side chains of Y109, Q111, Y124, and E126 (as indicated) and immobilized H_2O (red spheres) on the floor of the hydrophobic Sfh1 PL binding pocket. Bound PtdCho is also shown, and the *sn*-2 acyl chain C5 position is highlighted.

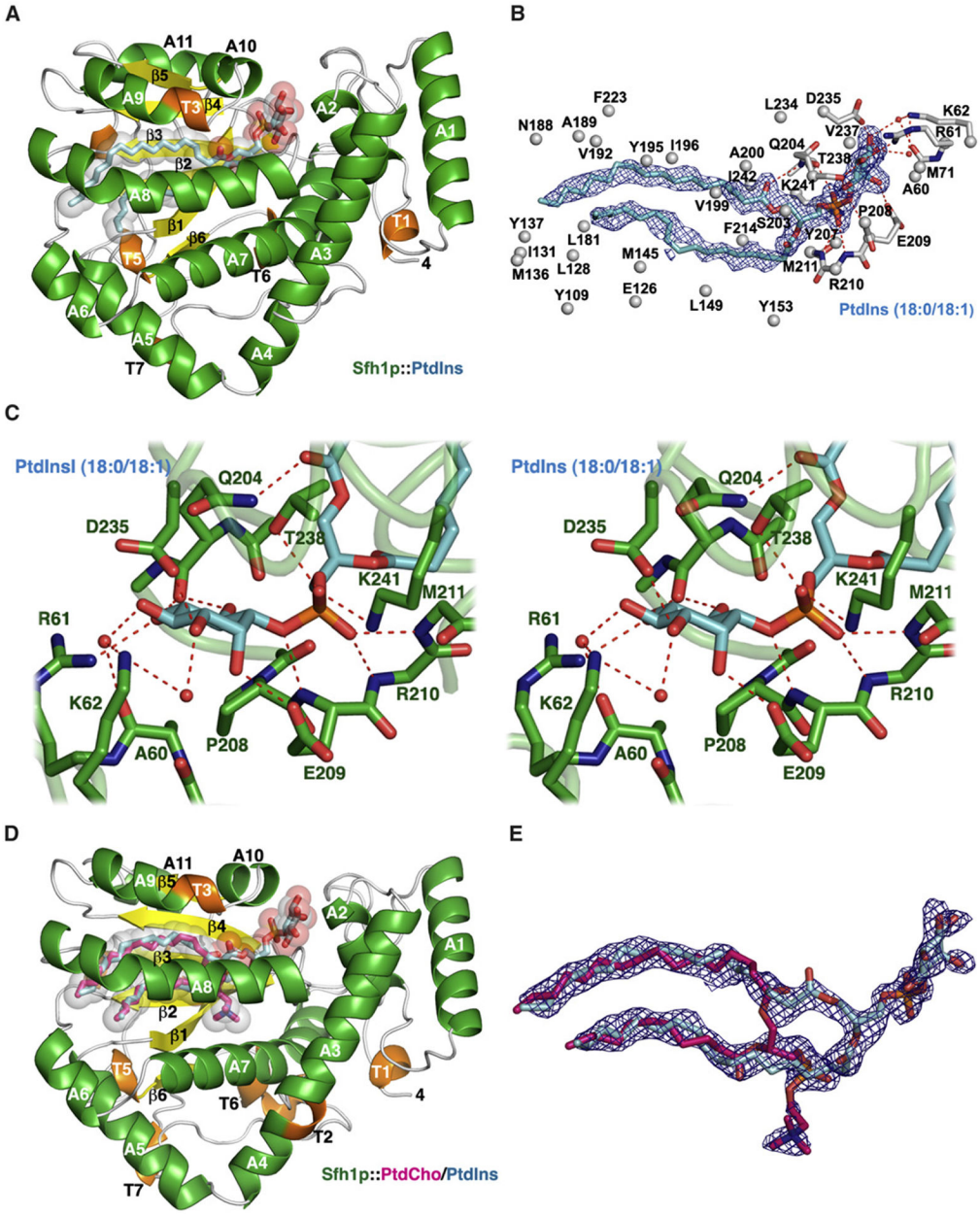

Figure 3. Structure of the Sfh1::PtdIns Complexes

(A) Structure of the Sfh1::PtdIns complex with PtdIns rendered in cyan as sticks and transparent spheres.

(B) $2F_o - F_c$ annealed omit electron density (contoured at 1σ) for bound 18:0/18:1 PtdIns. Residues within 4.2 Å of bound PtdIns are shown as white spheres. Residues that coordinate the PtdIns moiety are shown as sticks with H bonds represented as dashed lines.

(C) Stereoview of critical PtdIns headgroup interactions with Sfh1.

(D) Position of both PtdCho and PtdIns within the fold.

(E) $2F_o - F_c$ annealed omit electron density (contoured at 1σ) for bound 18:0/18:1-PtdIns and 16:0/18:1-PtdCho derived from the mixed crystal.

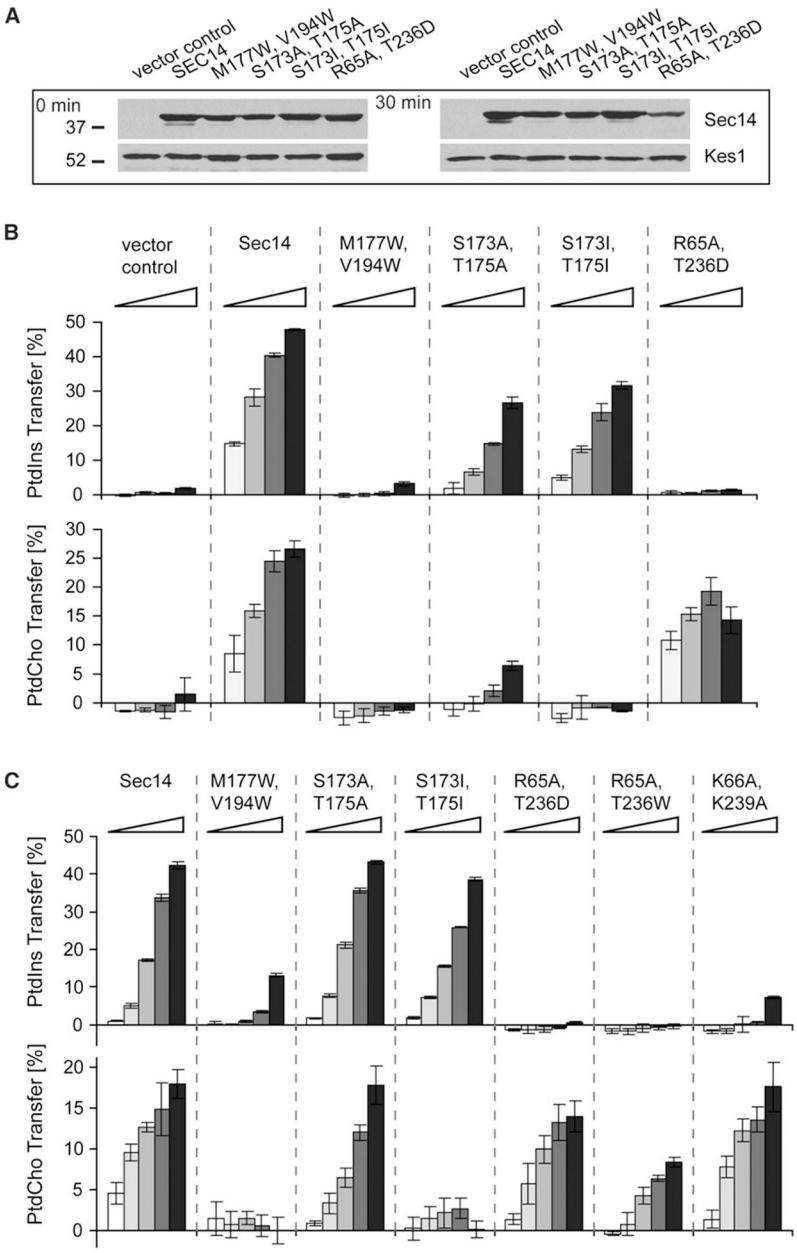

Figure 4. Biochemical Validation of Structure-Based Mutant Sec14 Derivatives

(A) Cytosolic fractions assayed in (A) were evaluated for Sec14 content by immunoblotting with an anti-Sec14 monoclonal antibody. Kes1 was evaluated as a control for proper normalization.

(B) PtdCho and PtdIns-transfer assay data are presented. Cytosols prepared from the *sec14Δ* strain CTY303 harboring the indicated YEp(*sec14*) plasmids were assayed. PtdIns-transfer assays used 0.12, 0.40, 1.20, and 4.0 mg cytosol. PtdCho-transfer assays employed 0.06, 0.20, 0.60, and 2.0 mg cytosol. YEp(*URA3*) and YEp(*SEC14*) derivatives were vector (negative) and positive controls. Average values and standard deviations are given (n = 3).

(C) Purified recombinant Sec14 proteins were assayed in a step series of 5-fold mass increases (0.004, 0.2, 1, 5, and 25 μg) for PtdCho- and PtdIns-transfer activity. Average values and standard deviations are given (n = 4).

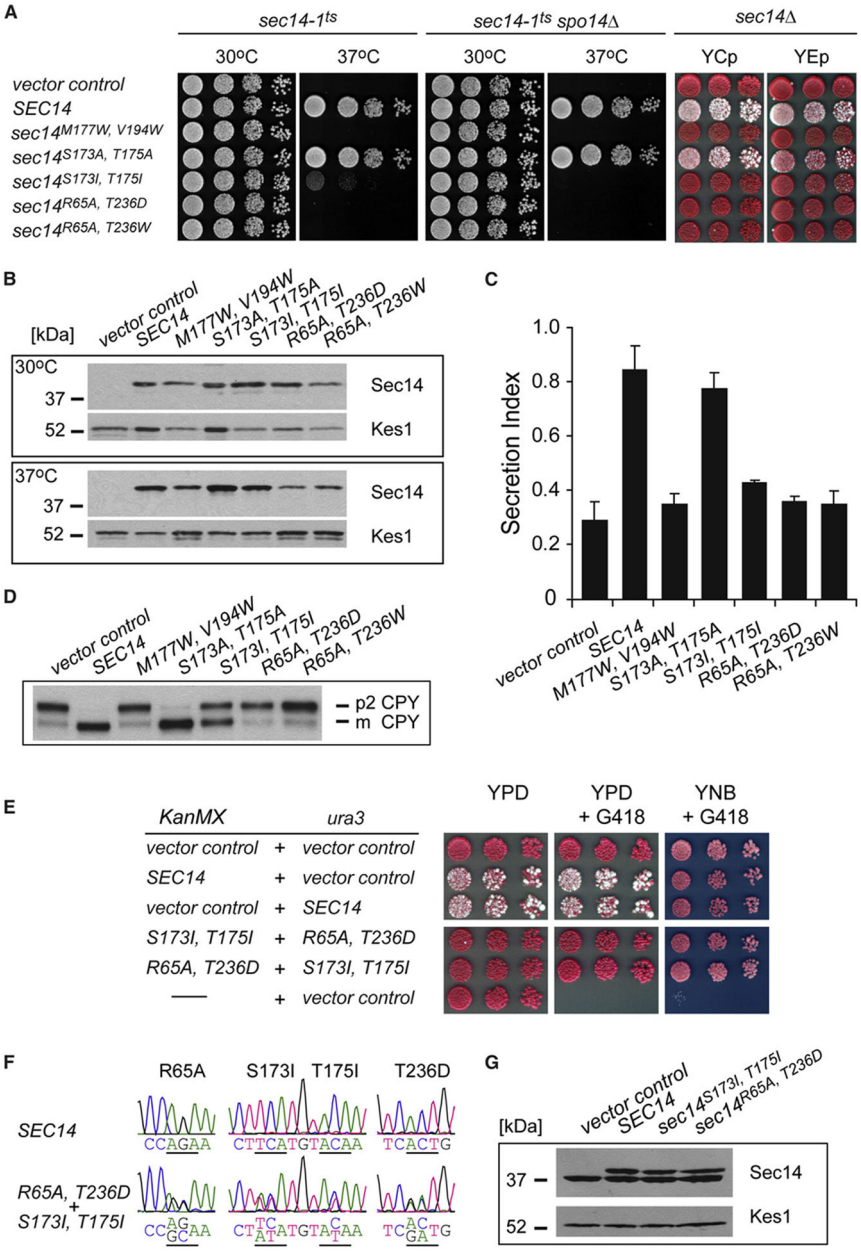

Figure 5. Functional Characterization of Structure-Based Mutant Sec14 Derivatives

(A) Left and middle panels, isogenic *sec14–1*^{ts} and *sec14–1*^{ts} *spo14Δ* yeast strains (identified at top) transformed with YCp plasmids carrying the designated *sec14* alleles (indicated at left) were spotted in 10-fold dilution series onto YPD agar plates and incubated at the restrictive temperature of 37°C. Rescue of growth defect reports functionality. YCp(*URA3*) and YEp(*SEC14*) derivatives served as vector (negative) and positive controls, respectively, in all experiments described in this Figure. Right panel, an *ade2 ade3 sec14Δ*/YEp(*SEC14, LEU2, ADE3*) yeast strain (strain CTY558; see Experimental Procedures) was transformed with the indicated YCp(*sec14, URA3*) or high-copy YEp(*sec14, URA3*) plasmids and dilution spotted onto YPD agar where all nutritional selection is removed. Functionality of mutant *sec14* product is manifested as appearance of white segregant

colonies that acquire leucine and histidine auxotrophies, signifying loss of parental YEp(*SEC14, LEU2, ADE3*). Retention of parental plasmid (i.e., nonfunctionality of the mutant *sec14*) is reported by red colony color (Phillips et al., 1999).

(B) Immunoblots of lysates prepared from *sec14–1^{ts}* yeast carrying the designated YCp(*sec14*) plasmids at 30°C (upper panel) and after 37°C challenge for 2 hr (lower panel). Equal amounts of total protein were loaded, and Sec14 and Kes1 (normalization control) were visualized with monoclonal antibodies specific for each (molecular mass standards at left).

(C) Invertase secretion indices are shown for isogenic *sec14–1^{ts}* strains transformed with low-copy YCp plasmids carrying the designated *sec14* alleles after a 2 hr shift to 37°C. Average values and standard deviations are given (n = 3).

(D) The indicated *sec14–1^{ts}*/YCp(*sec14*) strains were shifted to 37°C for 2 hr, and radiolabeled with [^{35}S] amino acids for 30 min followed by a 10 min chase. Vacuolar mCPY and TGN p2 CPY forms are identified at right.

(E) The *ade2 ade3 sec14Δ*/YEp(*SEC14, LEU2, ADE3*) yeast strain CTY558 was cotransformed with YCp(*myc-sec14 KanMX)* and YCp(*myc-sec14 URA3)* plasmids under conditions that select for parental YEp(*SEC14,LEU2,ADE3*). Transformants were dilution spotted onto YPD agar (relieves nutritional selection for *SEC14* plasmid, left panel), YPD agar supplemented with G418 (selects for *myc-sec14 KanMX*, middle panel), or selective media as used for the primary transformation (demands presence of all three plasmids, right panel). Functionality or nonfunctionality of combined expression of *myc-sec14* products from *KanMX* or the *URA3* low-copy plasmid is scored by loss or retention of parental *SEC14* plasmid, respectively. YEp(*SEC14*) loss events are manifested by appearance of white segregants (left and middle panels). YCp(*URA3*) and YCp(*KanMX*) plasmids served as mock controls.

(F) Nucleotide sequence of cDNA generated from yeast carrying both YCp(*myc-sec14^{R65A,T236D} KanMX*) and YCp(*myc-sec14^{S173I,T175I} URA3*) confirmed expression of mutant genes (lower panel). YCp(*myc-SEC14 KanMX*) and YCp(*URA3*) transformants were positive controls (upper panel). Base pair and amino acid substitutions are indicated (bottom and top, respectively). Nucleotide sequences were determined with *myc* tag-specific forward and *sec14*-specific reverse primers that do not amplify parental *SEC14* cDNA.

(G) Lysates prepared from CTY558 transformants carrying designated YCp(*myc-sec14 KanMX*) plasmids cultured at 30°C (in presence of G418) were probed for Sec14 antigen by immunoblotting. Loading was normalized by total protein. Kes1 was a normalization control. The *myc*-tagged *sec14* products and the parental plasmid *SEC14* product are identified.

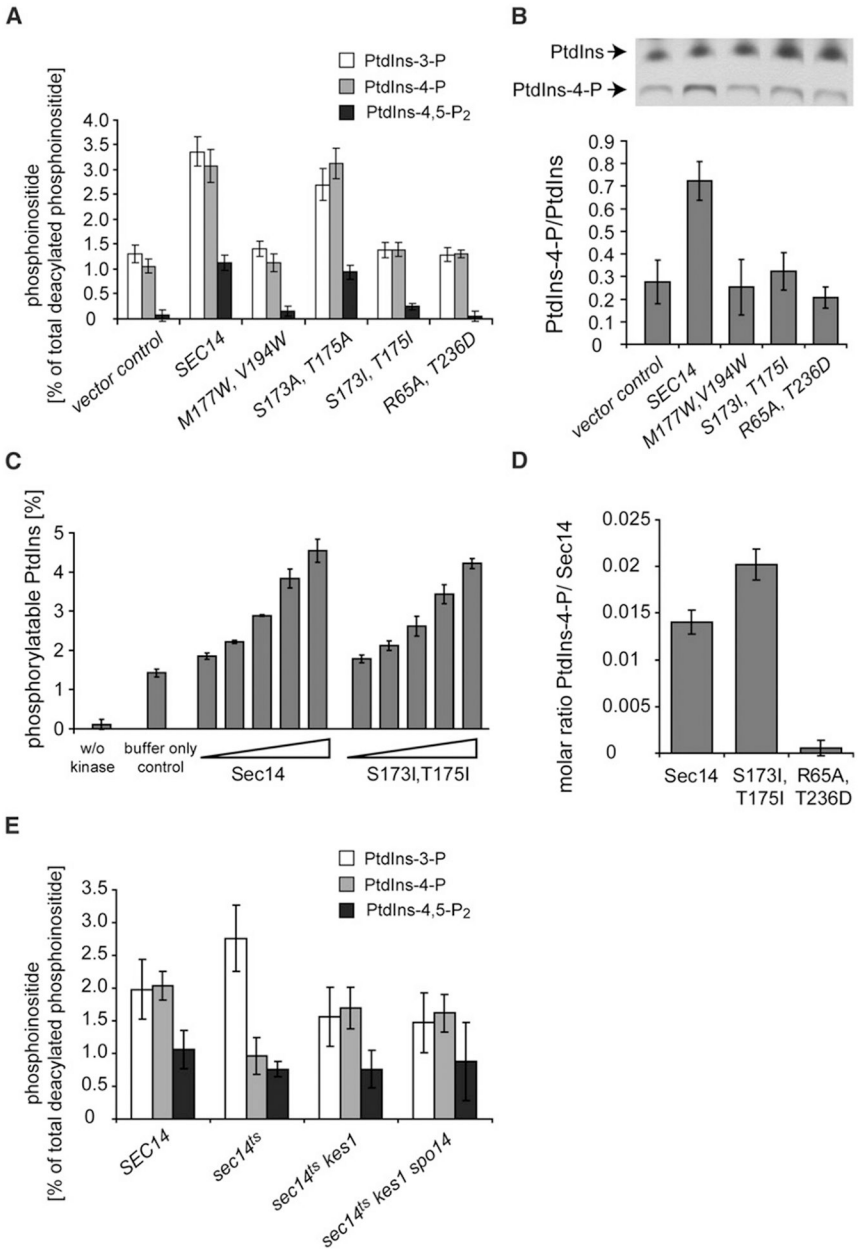

Figure 6. Sec14 PL Binding Activities and PIP Homeostasis

(A) PIP analyses. Derivatives of the *sec14Δ cki1* strain CTY303 carrying designated YCp plasmids were radiolabeled for 18 hr at 30°C with 20 μCi/ml [^{3}H]-Ins. Deacylated PIPs were quantified (see Experimental Procedures). PtdIns-3-P, PtdIns-4-P, and PtdIns(4,5)P_2 are as indicated. Average values and standard deviations are given (n = 4). YCp(*URA3*) and YCp(*SEC14*) derivatives served as negative and positive controls, respectively.

(B) Stt4 activity as a function of mutant *sec14* proteins. A *sec14–1^{ts} sac1–26* yeast mutant (CTY100) and isogenic derivatives expressing the indicated Sec14 proteins were radiolabeled to steady state with [^{3}H]-Ins and shifted to 37°C for 2 hr. PtdIns-4-P and other Ins-PLs were extracted, resolved by thin layer chromatography, and identified by cochromatography with radiolabeled standards, and Stt4-dependent PtdIns-4-P accumulation

was quantified as described (Phillips et al., 1999). The *URA3* and *SEC14* derivatives represented negative and positive controls, respectively. Average values and standard deviations are given (n = 4).

(C) In vitro PtdIns kinase stimulation. The indicated recombinant Sec14 proteins were assayed in a step series of 3-fold mass increases (0.03, 0.09, 0.81, and 2.43 μg) in reactions containing 2.5 μg PtdIns 4-OH kinase, PtdIns:PtdCho liposomes, and [γ^{32}P]-ATP. Data are plotted as percentage of total achievable PtdIns-4-P signal as determined in mixed micelle assays where Triton X-100 (0.4%) was incorporated into the system (see Experimental Procedures). Average values and standard deviations are given (n = 3).

(D) In situ phosphorylation of Sec14-bound PtdIns. Sec14 and mutant derivatives were loaded with PtdIns and repurified from PtdIns liposomes on cobalt affinity resin followed by extensive washing and dialysis. For the in situ kinase reaction, 1.5 μg Sec14 was used and processed as described for in vitro kinase assays that employed liposomes. Average values and standard deviations are given (n = 3).

(E) PIP analyses in *sec14 kes1* mutants. Isogenic derivatives of the *SEC14* (CTY182), *sec14–1^{ts}* (CTY1–1A), *sec14–1^{ts} kes1* (CTY159), and *sec14–1^{ts} kes1 spo14Δ* (CTY1098) were radiolabeled for 18 hr at 30°C with 20 μCi/ml [^{3}H]-Ins and then shifted to the restrictive temperature of 37°C for 2 hr. Deacylated PIPs were quantified, and PtdIns-3-P, PtdIns-4-P, and PtdIns(4,5)P_2 are as indicated (n = 5). *SEC14* and *sec14–1^{ts}* strains were positive and negative controls, respectively. The *sec14–1^{ts} kes1* and *sec14–1^{ts} kes1 spo14Δ* mutants exhibited elevated PtdIns-4-P relative to *sec14–1^{ts}* controls. Average values and standard deviations are given (n=5; $p < 0.01$ and $p < 0.02$, respectively).

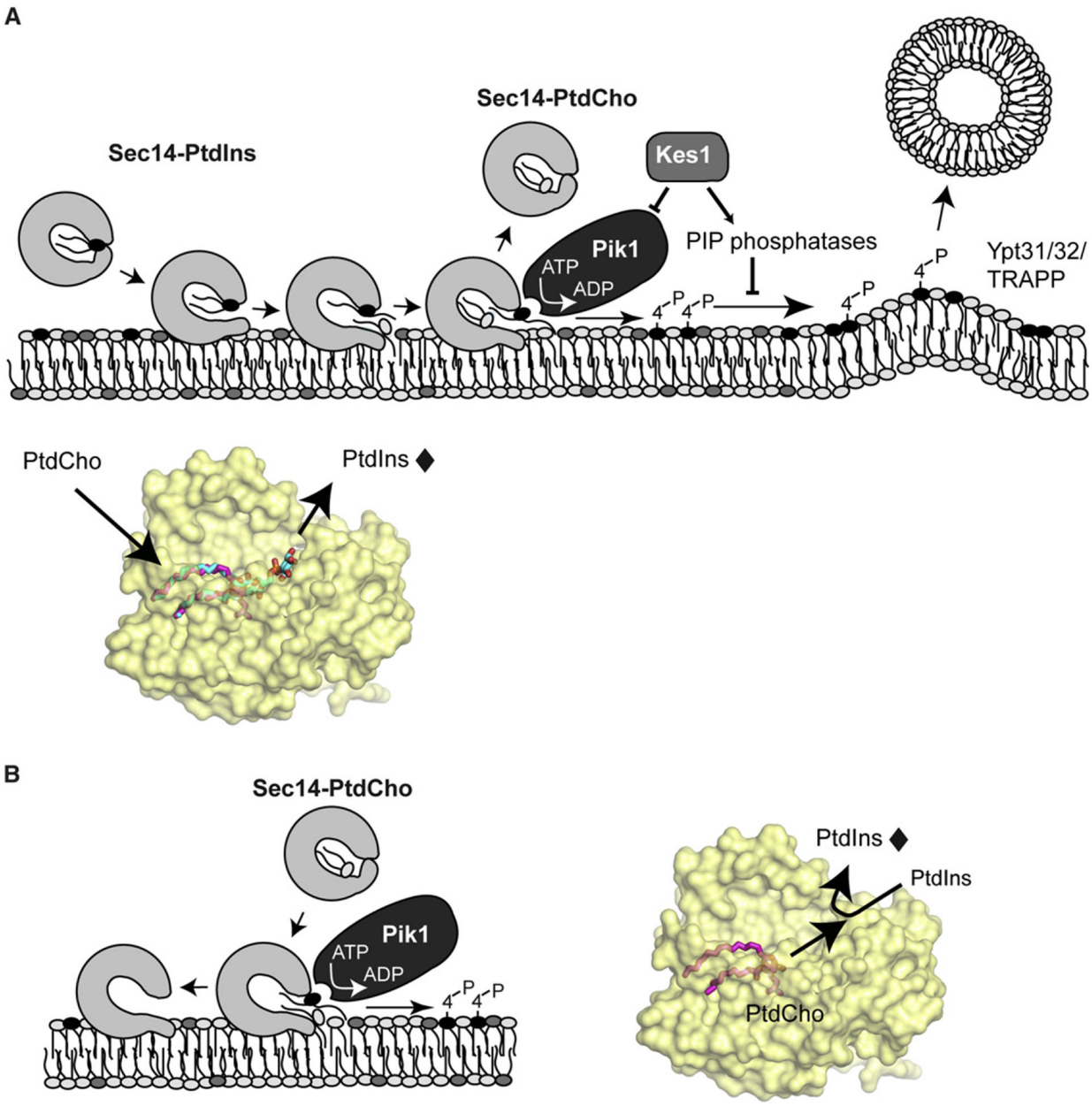

Figure 7. Sec14 Function in PIP Homeostasis in the Yeast TGN

A two-ligand Sec14 priming model for PtdIns presentation to PtdIns kinases is shown.

(A) Heterotypic exchange results in PtdCho entering the Sec14 pocket and ejecting bound PtdIns through an unobstructed portal (bottom panel). Egress occurs headgroup-first, and the exposed intermediate (◆) is highly susceptible to modification by Pik1 PtdIns 4-OH kinase in the TGN. This potentiation of Pik1 activity overcomes the net inhibitory effects of Kes1 and likely couples to the Ypt31/32 pathway for vesicle biogenesis.

(B) Alternatively, slow egress of bound PtdCho interferes with entry of an invading PtdIns and delays it as a partially incorporated and exposed intermediate (◆) that is vulnerable to Pik1 modification. Completion of PtdCho unloading generates an apo intermediate that

reloads with PtdIns or PtdCho (left panel). This mechanism suggests invading PtdIns and the leaving PtdCho collide in spatially overlapping entry/exit portals (right panel).

Mol Cell. Author manuscript; available in PMC 2021 January 14.

Table 1.

Data Collection and Refinement Statistics

	Sfh1::PtdEtn	**Sfh1::PtdIns**	**Sfh1::PtdCho**	**Sfh1::PtdIns/PtdCho**
Resolution (highest shell) (Å)	1.90 Å (1.90–1.97)	1.86 Å (1.86–1.97)	2.00 Å (2.07–2.00)	2.03 Å (2.10–2.03)
Space group	$P2_12_12_1$	$P2_12_12_1$	$P2_1$	$P2_12_12_1$
Unit cell dimensions	a = 49.5, b = 71.3, c = 99.8 α = γ = β = 90.0	a = 50.2, b = 71.4, c = 91.2 α = γ = β = 90.0	a = 49.4, b = 71.3, C = 115.2 α = β = 90.0, γ = 94.1	a = 49.4, b = 72.9, c = 97.6 α = γ = β = 90.0
Number of reflections	27,203	27,304	53,191	21,696
R_{sym} (highest shell)[a]	8.8% (30.8%)	9.6% (36.7%)	11.9% (35.5%)	8.0% (24.7%)
Completeness (highest shell)	96.8% (98.9%)	99.5% (98.7%)	97.4% (97.8%)	95.8% (93.2%)
Average redundancy (highest shell)	5.8 (5.4)	4.7 (4.0)	2.7 (2.6)	4.1 (3.9)
I/σ	17.7 (5.0)	15.1 (4.8)	10.2 (3.8)	16.8 (5.0)
Monomers per asymmetric unit (AU)	1	1	2	1
Number of protein atoms/AU	2520	2523	5040	2520
Number of ligand atoms/AU	44	59	52	103
Number of waters/AU	246	265	409	231
$R_{working}$[b] (R_{free}[c])	20.4% (22.1%)	19.1% (23.3%)	20.5% (24.2%)	20.1% (23.8%)
Average B factors (Å^2)				
Protein	23.5	22.4	24.2	30.8
Ligand	31.5	35.9	43.4	31.3
Water	30.7	32.8	33.0	35.5
Ion	–	54.3	61.0	–
Rmsds				
Bond lengths (Å)	0.006	0.005	0.006	0.005
Bond angles (°)	1.2	1.011	1.4	1.011
PDB ID	3B74	3B7N	3B7Q	3B7Z

[a] $R_{sym} = \Sigma|I - \langle I\rangle| / \Sigma|I|$, where I is the observed intensity and $\langle I\rangle$ is the average intensity of several symmetry-related observations.

[b] $R_{working} = \Sigma||F0| - |F_C||/\Sigma|F_O$, where F_O and F_C are the observed and calculated structure factors, respectively.

[c] $R_{free} = \Sigma||F_O| - |F_C|| / \Sigma|F_O|$ for 7% of the data not used at any stage of the structural refinement.